# Methane Combustion Kinetics over Palladium-Based Catalysts: Review and Modelling Guidelines

Roshni Sajiv Kumar, Joseph P. Mmbaga, Natalia Semagina ![ORCID] and Robert E. Hayes *

Department of Chemical and Materials Engineering, University of Alberta, Edmonton, AB T6G 2V4, Canada; sajivkum@ualberta.ca (R.S.K.); jmmbaga@ualberta.ca (J.P.M.); semagina@ualberta.ca (N.S.)
* Correspondence: hayes@ualberta.ca

**Abstract:** Fugitive methane emissions account for a significant proportion of greenhouse gas emissions, and their elimination by catalytic combustion is a relatively easy way to reduce global warming. New and novel reactor designs are being considered for this purpose, but their correct and efficient design requires kinetic rate expressions. This paper provides a comprehensive review of the current state of the art regarding kinetic models for precious metal catalysts used for the catalytic combustion of lean methane mixtures. The primary emphasis is on relatively low-temperature operation at atmospheric pressure, conditions that are prevalent in the catalytic destruction of low concentrations of methane in emission streams. In addition to a comprehensive literature search, we illustrate a detailed example of the methodology required to determine an appropriate kinetic model and the constants therein. From the wide body of literature, it is seen that the development of a kinetic model is not necessarily a trivial matter, and it is difficult to generalize. The model, especially the dependence on the water concentration, is a function of not only the active ingredients but also the nature of the support. Kinetic modelling is performed for six catalysts, one commercial and five that were manufactured in our laboratory, for illustration purposes.

**Keywords:** catalytic combustion; methane; kinetic models; mechanism

## 1. Introduction

Catalytic combustion is a flameless combustion that has received considerable attention over the last few decades, although it has been reported on for over one hundred years [1–3]. The key advantages of catalytic combustion compared to conventional combustion are the elimination of the standard flammability limits and the ability to combust the reactants at a lower temperature. There are several factors that have been driving the interest in the catalytic combustion of methane in recent years, most of which are related to the solution of environmental problems. Methane is well known as a strong greenhouse gas, and there have been significant efforts made to reduce its emission, especially from such sources as the oil and gas industry, agriculture, and landfills. There is also an interest in the use of methane as an alternative fuel in internal combustion engines (ICEs) as a replacement for diesel or gasoline. Changing the fuel results in a large reduction in the emission of greenhouse gases, provided that the methane that is not burned in the engine is successfully destroyed in a catalytic converter. Even if a large part of the transportation energy is able to transition to electric vehicles, there will remain a need for ICEs in many applications. The aforementioned applications relate to what is referred to as secondary applications. There are also applications where the desire is to produce power from the combustion of natural gas, usually in a gas turbine, but to do so at a lower temperature than conventional homogeneous combustion [4–6].

The broad range of applications alluded to in the foregoing implies a plethora of possible reactor feed conditions. Generally speaking, the feed type can be divided into those containing significant quantities of water (wet feed) and those that do not (dry feed).

It is often the case that the methane concentration is low, and there is an excess of oxygen (lean feed). Many fugitive streams and those from compression ignition (CI) engines fall into this category. On the other hand, the feed may be stoichiometric, as for spark ignition (SI) engines, or even methane-rich, as for some fugitive emission streams. Furthermore, the feed temperature can be at ambient or elevated temperature. In addition to the nature of the feed, another key factor is the allowable or possible operating temperature of the catalyst section in the reactor. In some cases, the internal recuperation of energy may be used to maintain a high reactor temperature even with a low feed temperature [7–11].

Many catalysts have been used for hydrocarbon combustion in general and for methane in particular [12]. Several metals have been reported, both non-noble (or earth common) as well as metals from the platinum group metals (PGMs), especially platinum and palladium. With cost being a major factor in catalyst selection, there is obviously a large interest in the more earth-abundant and lower-cost metals [13–21]. A common disadvantage of earth common metals is that they have a lower activity, which can then result in the reactor having a large physical footprint. Furthermore, a lower activity implies a higher reactor operating temperature, which is not always desirable. Because of their higher activity, PGMs are more commonly employed in applications where either or both a small reactor and low ignition temperature are desired [22–26].

Platinum is one of the major PGM components of the standard automotive catalytic converters and is often considered to be the most effective choice for the combustion of non-methane hydrocarbons. It has, however, also been reported in methane combustion applications, with the catalyst taking various forms [27–36]. Although platinum does play a role, the most widely used PGM catalyst for methane combustion is palladium, and research on this metal likely accounts for the majority of papers extant on this subject.

As with most catalytic systems, the role of the support is also important, and its selection can affect both the catalytic mechanism and activity and the resulting rate equation, as reported in, for example, references [37–41]. Reported supports include, for example, alumina [42–49], zirconia [50–54], silica [55–57], aluminosilicates [58], cobalt oxide [59,60], ceria [61,62], nickel compounds [63], and tin [64,65]. In addition to the choice of support, the preparation method [66–68] and the use of promoters [69–71] can also have a significant impact on the catalytic activity.

Using combinations of PGMs for methane combustion catalysts is common, and such additions include rhodium [72–76] and gold [77–79]. By far, the most common combination is palladium and platinum, with example references being [80–93].

It is clear that with this large variety of possible catalysts, even restricting ourselves to those based on PGMs, there exists the possibility for different rate expressions and reaction mechanisms. In this paper, we provide a review of kinetic modelling studies that have been reported in the literature with a view to summarizing the current state of knowledge. The focus is on the type of catalysts typically used for emission control applications, rather than those for power applications, which are usually carried out at elevated temperatures. We then present the results of a detailed investigation into kinetic studies for some methane oxidation catalysts with PGMs as the primary active ingredient. We use a leading commercial catalyst as a benchmark and then show results from five PGM catalysts that were prepared in our own laboratories. This paper should make a valuable contribution to those contemplating kinetic studies for these types of catalysts.

## 2. Review of Reaction Mechanism and Kinetic Models

As noted in the Introduction, the primary active ingredient in catalysts used to promote the oxidation of methane is often palladium. The active form of the metal is palladium oxide (PdO), and it has been shown [94,95] that PdO is readily formed when supported Pd is heated in an oxygen environment above temperatures of 523 to 573 K. Although PdO is more active in the oxidation of methane than Pd, PdO begins to decompose to form Pd at higher temperatures [96]. The transition temperature depends on the oxygen partial pressure above the catalyst, and at 20% oxygen, the transition temperature is

about 1023 K [3] and decreases as the oxygen partial pressure is reduced. This transition temperature can become very important when methane is combusted under stoichiometric conditions, such as what often occurs in a spark ignition natural gas engine.

Many studies have been carried out to elucidate the reaction mechanism and thus propose rate models for PGM-based methane combustion in the presence and absence of water. Some early work is reviewed in [22]. The reaction is not straightforward to study, and the catalyst activity can be a strong function of the support type, preparation method, and operating history [97,98].

First-principle investigations [99] reported that dry methane combustion on the PdO(101) facet occurred via two routes depending on the temperature; in the 500–630 K range, C-H bond cleavage occurred via reaction with the OH groups, while in the 900–1000 K temperature range, C-H bond cleavage occurred through reaction with the lattice oxygen atoms. At the higher temperature ranges, the rate-determining step (RDS) was proposed to be the dissociative adsorption of methane on the PdO surface, while in the lower temperature ranges, water adsorption on the undercoordinated Pd sites was the RDS [97]. Utilizing microcalorimetry studies, Xin et al. [100] proposed similar conclusions, with methane combustion following a pseudo-first-order reaction in terms of methane kinetics for dry methane combustion on PdO. Contrary to these findings, Specchia et al. [101] proposed that dry methane combustion on $PdO/Ce_xZr_{1-x}O_2$ occurred via a Mars–van Krevelen mechanism. In a study by Müller et al. [102], dry methane combustion over $^{18}O$-labelled $ZrO_2$-supported PdO was proposed to occur partially via a redox Mars–van Krevelen mechanism. However, the overall conversion was found to be influenced by the coaction between the surface reaction of the adsorbed reactants and the redox mechanism [102]. Following this hypothesis, a study by Fujimoto et al. [52] on the kinetics of dry methane combustion at low temperatures on the $Pd/ZrO_2$ catalyst characterized by the Mars–van Krevelen mechanism detected the involvement of methane activation in site pairs comprising Pd, which functions as an oxygen vacancy and $PdO_x$ that serves as a source for the oxygen atoms. Methane was found to be dissociatively adsorbed on metallic Pd, thereby producing H and $CH_x$ species, while oxidation occurred on the adjacent PdO [53,103].

Wet methane combustion on Pd-based catalysts has been reported to be independent of $O_2$ and $CO_2$ concentrations and was determined to have a reaction order of 1 and $-1$ for methane and water, respectively [52,104]. The RDS for wet methane combustion on monometallic Pd at lower temperatures (below 723 K) was determined to be water desorption from the catalyst surface [105], while at higher temperatures, the RDS was determined to be methane activation on the Pd sites [52]. Regarding the mechanism for methane combustion, using a $PdO_x/ZrO_2$ catalyst, Fujimoto et al. [52] reported that the reaction occurred in three steps. Initially, methane molecules were physically adsorbed onto vacant metallic Pd sites, followed by sequential hydrogen-atom abstraction from the adsorbed methane backbone, which resulted in the formation of surface hydroxyl. The proposed rate-determining step for this reaction was determined to be the H-atom abstraction from the methane molecule when the OH* species were the most abundant surface intermediate species [52]. Later, it was proposed by Ribeiro et al. [106] and Burch et al. [107] that the decomposition of the surface hydroxyl (Pd-OH) was the determining factor for methane activation.

Based on the above mechanistic observations, the rate expression for the catalytic combustion of methane for the dry case is often reported in the form of a power-law-type equation as follows:

$$(-r_{CH_4}) \;=\; k[CH_4]^m[O_2]^n \tag{1}$$

As noted above, water has a strong effect on the reaction rate. The inhibition effect of water may be caused by the transition of palladium oxide to palladium hydroxide [106,108,109] according to the following reaction:

$$PdO \;+\; H_2O \;\rightleftharpoons\; Pd(OH)_2 \tag{2}$$
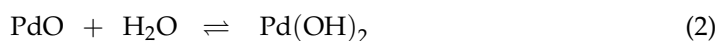
Although Pd(OH)$_2$ has been reported to decompose to PdO at 520 K [110], it has been suggested that the ability of the support to retain water can stabilize Pd(OH)$_2$ at higher temperatures [37,109].

The classical power law model incorporating the strong inhibition effect of water for Pd-based catalysts was proposed as follows [106,111,112]:

$$(-r_{CH_4}) = k[CH_4]^m[O_2]^n[H_2O]^l \tag{3}$$

The order of the reaction with respect to methane is often reported to be one or slightly less, whilst the order of reaction with respect to oxygen is zero or close to zero [111,112], although other orders have been reported [113,114]. Variation in the values of *n* and *m* for such a power law model can be explained using the theory of kinetics over non-uniform surfaces, where $n + m = 1$. DFT studies by Qi et al. [115] revealed that for dry methane combustion on a Pd catalyst, the RDS was the dissociation of methane on matched pair sites. The authors proposed a rate equation in the form of Equation (1), with $m = 1$, $n = 0$ and $l = -1$.

There is a lack of agreement on the effect of carbon dioxide on methane oxidation over palladium. Some investigators [37,108,109] reported negligible inhibition, whilst others [106] reported significant inhibition with about 0.5 volume % carbon dioxide.

Utilizing the Mars–van Krevelen mechanism, Golodets et al. [116] proposed a rate equation for methane oxidation incorporating the water inhibition term as follows:

$$(-r_{CH_4}) = \frac{k_1[CH_4]}{1 + k_2\left\{\frac{[CH_4]}{[O_2]}\right\} + K_3[H_2O]} \tag{4}$$

Mezaki and Watson [117] proposed a simplified rate equation for the scenario if adsorbed water was the most abundant surface intermediate, which is as follows:

$$(-r_{CH_4}) = \frac{k_1[CH_4]}{1 + K_3[H_2O]} \tag{5}$$

Modelling studies by Hayes et al. [104] for methane combustion over Pd catalysts in the presence and absence of water revealed that the water inhibition term had to be included in the rate equation, as illustrated in Equation (5). In another study by Kikuchi et al. [118], the same rate expression as in Equation (5) was utilized to model wet methane combustion on Pd/Al$_2$O$_3$ and Pd/SnO$_2$ catalysts and found a good agreement between the modelling and experimental results.

Several catalytic methane combustion studies on Pd/Al$_2$O$_3$ catalysts revealed a first order to CH$_4$ and a negative first order to H$_2$O [106,119,120]. Utilizing a steady-state mole balance equation, depicted in Equation (6), Alyani et al. [120] revealed that the activation energy associated with splitting the first C-H bond for Pd/Al$_2$O$_3$ was in the range of 60 to 72 kJ/mol, while the heat of water adsorption was determined to be around −81 kJ/mol.

$$\frac{dX_{CH_4}}{d\left(\frac{W}{F_{CH_4}^0}\right)} = \eta \frac{k_s C_T^2 P(1 - X_{CH_4})y_{CH_4}^0}{1 + K_{H_2O}P(\alpha_{H_2O} + 2X_{CH_4})y_{CH_4}^0} \tag{6}$$

Kinetic studies for lean-burn wet methane combustion on SnO$_2$-supported Pd-based catalysts by Kikuchi et al. [118] revealed that the catalyst followed a rate equation similar to that illustrated in Equation (5). In this case, the activation energy was determined to be around 111 kJ/mol, and the heat of water adsorption value was −31 kJ/mol [117]. Contrary to this, the wet methane combustion studies by Kumar et al. [121] on a Pd/SnO$_2$

catalyst revealed a partial order of −0.11 to water. Considering the partial order to water, the authors proposed an additive reaction rate equation, as depicted below [121].

$$(-r_{CH_4}) \;=\; k_1[CH_4] \;+\; \frac{k_2[CH_4]}{[H_2O]} \tag{7}$$

The first site was considered to be unaffected by water, while the second site was considered to be affected by water with a reaction order of −1 to it. Keeping the observed activation energy on the site affected by water similar to that observed in the case of the conventional $Pd/Al_2O_3$ catalyst, the activation energy on the site unaffected by water was determined to be 108 kJ/mol [120]. Similar studies by Keller et al. [122] revealed an activation energy ($E_{a0}$) of 144 kJ/mol and 117 kJ/mol for the $Pd/Al_2O_3$ catalyst and $Pd/SnO_2$ catalyst, respectively. However, the authors utilized a rate equation that incorporated an inhibition factor, as depicted below.

$$(-r_{CH_4}) \;=\; \frac{k_1[CH_4]}{1 + K_3[H_2O]^\beta} \tag{8}$$

While Equation (8) is similar to Equation (5), Keller et al. determined that the order to water, that is, the value of β for the $Pd/Al_2O_3$ catalyst and $Pd/SnO_2$ catalyst, was 1.99 and 0.87, respectively [122]. Studies by Nasr et al. [123] for lean wet methane combustion on a $Pd/Co_3O_4$ catalyst also revealed a partial order of −0.37 to water. The authors proposed a rate model with additive contributions from the Pd and Co counterparts as follows:

$$(-r_{CH_4}) \;=\; k_1[CH_4] \;+\; \frac{k_2[CH_4]}{[H_2O]} \;=\; \left(k_1 + k_2\frac{1}{[H_2O]}\right)[CH_4] \;=\; k^*[CH_4] \tag{9}$$

Their kinetic study revealed that the higher water tolerance on the $Co_3O_4$-supported catalyst was due to synergism resulting from strong metal–support interactions between Pd and Co [123].

Several studies have been conducted to define rate equations for methane combustion on Pt-only catalysts as well [124–126]. While Pt is known to be less active than Pd/PdO for methane combustion under dry feed conditions, Pt is found to be active to catalyze methane combustion under wet feed conditions in its metallic state [23,127]. Considering the first H-atom abstraction from the C-H backbone by chemisorbed oxygen on Pt as the rate-determining step [115], the generally accepted rate equation for methane combustion on Pt-based catalysts is illustrated as follows [126,128]:

$$(-r_{CH_4}) \;=\; k[CH_4] \tag{10}$$

Utilizing a rate equation like Equation (3), DFT studies by Qi et al. [115] for methane combustion on Pd-Pt catalysts with varying Pd:Pt ratios revealed reaction orders of −1.05, −0.98, and −0.79 to water for $Pd_{0.75}Pt_{0.25}$, $Pd_{0.5}Pt_{0.5}$, and $Pd_{0.25}Pt_{0.75}$ catalysts, respectively. Similar studies by Abbasi et al. [124] for bimetallic Pd:Pt catalysts in the presence and absence of water revealed a rate equation as follows:

$$(-r_{CH_4}) \;=\; \frac{k_1[CH_4]}{(1 + K_2[CH_4] + K_3[H_2O])^n} \tag{11}$$

$K_2$ essentially had a value of zero, and the value of *n* was determined to be 1 [124]. In another study by Habibi et al. [129] for $SiO_2$-encapsulated Pd-Pt catalysts, the authors revealed that the catalyst followed different rate equations in the presence and absence of water. While under dry feed conditions, the catalyst followed a rate equation as that of Equation (5), under wet feed conditions, the catalyst followed a rate model given by [29].

$$(-r_{CH_4}) \;=\; \frac{k_1 K_2[CH_4]}{(1 + K_2[CH_4])K_3[H_2O]} \tag{12}$$

Equation (12) was proposed by accounting for the water-inhibiting oxygen exchange effect on the support surface [129]. Lean-burn wet methane combustion kinetic studies on $Al_2O_3$ and $SnO_2$-supported Pd:Pt catalysts by Kumar et al. [121] revealed that both catalysts exhibited a −1 order to water. While the $Pd/SnO_2$ catalyst exhibited a partial order to water, different mechanisms of Pt and $SnO_2$ actions resulted in bimetallic catalysts exhibiting a −1 order to water. Interestingly, while the $Pd-Pt/Al_2O_3$ catalyst and $Pd-Pt/SnO_2$ catalyst revealed similar activation energies in the range of 134 kJ/mol, the presence of different active sites on either catalyst resulted in the $Pd-Pt/SnO_2$ catalyst exhibiting a higher turnover frequency, almost two-fold in magnitude as that observed on the $Pd:Pt/Al_2O_3$ catalyst [121]. Utilizing a rate equation like that of Equation (3), Yang et al. [130] revealed that while the $Pd/Al_2O_3$ catalyst exhibited a −1 order to water, the $Al_2O_3$-supported Pd-Pt catalyst exhibited an order of −0.23 to water. The authors also revealed that the addition of Pt resulted in a reduction in the activation energy from 127 kJ/mol in the Pd catalyst to 58 kJ/mol in the Pd-Pt catalyst in the presence of water [130].

It has also been observed that there can be a significant change in the activation energy of the reaction at higher temperatures. An early work [22] on methane oxidation over Pd catalysts in the temperature range of 500 to 800 K reported a sharp change in the activation energy of the reaction. The temperature at which the change occurred varied from 654 to 720 K and was a function of support material and reactant concentration. The low-temperature range activation energy varied from 75 to 95 kJ/mol and decreased to a value between 23 and 45 kJ/mol at high temperatures. In another work [131], an activation energy of 131 kJ/mol was reported below 770 K and 19 kJ/mol at higher temperatures. The authors attributed the decline to heat and mass transfer effects, although these effects are likely to be the major cause [132].

Sakai et al. [133] studied a Pd catalyst for methane combustion and observed a transition at about 690 K, with the activation energy dropping from 76.5 kJ/mol to 61 kJ/mol. Liu et al. [134] also observed a change in apparent activation energy. In their model, all heat and mass transfer steps were accounted for explicitly. These observations for the transition of methane catalytic oxidation activity are summarized in Table 1. Finally, in [10], the transition from 104 kJ/mol to 47.5 kJ/mol was observed to happen at about 811 K. In this work, all heat and mass transfer effects were explicitly accounted for. Clearly, there is some complexity and variation with this reaction.

**Table 1.** Temperature dependence of the activation energy for the palladium-catalyzed oxidation of methane based on first-order kinetics.

| Reference | Activation Energy, kJ/mol | | Transition Temperature, K |
|-----------|---------------------------|---------------------------|---------------------------|
| | Low-Temperature Region | High-Temperature Region | |
| [22] | 75–95 | 23–45 | 654–720 |
| [131] | 131 | 19 | 770 |
| [133] | 129 | 35 | 874 |
| [134] | 76.5 | 61 | 690 |
| [104] | 47.5 | 104 | 811 |

## 3. Experimental Program

### 3.1. Catalyst Details

As mentioned in the Introduction, we tested and compared the performance of six catalyst formulations. The first catalyst tested was a commercial methane combustion catalyst provided in the form of a wash-coated monolith. The properties of the monolith used in calculating the reactor loading are given in Table 2. The supplied wash-coated monolith was crushed and sieved to a size between 44 and 63 microns (between 230 and 325 mesh size). It was then calcined in air at 550 °C for 16 h. This sample is subsequently referred to as the fresh catalyst. The standard target catalyst reactor loading was to have 1.2 mg of PGMs in the reactor. Based on the PGM loading provided by the manufacturer, and using the numbers in Table 2, a piece of monolith contains about 0.675% by mass PGM.

Therefore, to achieve 1.2 mg of PGMs in the reactor, we should have 0.18 g of the crushed monolith, which we rounded to 0.2 g.

**Table 2.** Properties of the wash-coated catalytic monolith used in this study.

| | |
|---|---|
| Cell density | 400 CPSI |
| Substrate density | 1650 kg/m$^3$ |
| Substrate volume fraction | 25% |
| Washcoat density | 1100 kg/m$^3$ |
| Washcoat volume fraction | 0.12 |
| Palladium loading in monolith (assumed) | 100 g/ft$^3$ |

We now consider the catalysts made in the lab. Five catalysts were compared in this set, all for fresh catalysts under dry conditions. The details of the catalyst compositions are shown in Table 3. All catalysts contain 1 weight % of PGMs, which were Pd and Pt in equal molar amounts. The preparation of catalysts 3 and 6 is described in reference [121] and that for 2, 4, and 5 is given in reference [135,136]. These references also give the results of the characterization of these catalysts and the other experimental conditions present. They also present in-depth kinetic investigations of the kinetic modelling of lean wet methane combustion for fresh and hydrothermally aged catalysts in the presence of 5 and 10% by volume of water. In the current work, we present and compare the kinetic modelling of dry methane combustion over fresh catalysts only.

**Table 3.** Catalyst compositions for the five catalysts made in the laboratory.

| Catalyst Number | Catalyst Formulation |
|---|---|
| 2 | Pd:Pt supported on $Co_3O_4/SnO_2$ |
| 3 | Pd:Pt supported on $SnO_2$ |
| 4 | Pd:Pt supported on $Co_3O_4$ |
| 5 | Pd:Pt supported on $Co_3O_4/\gamma$-$Al_2O_3$ |
| 6 | Pd:Pt supported on $\gamma$-$Al_2O_3$ |

*3.2. Experimental Reactor System*

The experimental procedures used were similar to those described elsewhere [124,136], and the basic description is included here for completeness. Catalyst activity measurements were made using a small reactor system consisting of a reactor, furnace, thermocouples and temperature controller, flow meters, and gas and water supply, as shown in Figure 1. The reactor had an inner tube of 0.76 cm (3/8″) diameter with an outer sleeve of 2.22 cm (7/8″) diameter, both made from 316 stainless steel. The role of the outer sleeve was to provide a constant temperature along the wall of the reactor. The reactor assembly was installed inside of a tubular furnace. The catalyst was located in the middle of the reactor, and quartz wool was placed before and after the catalyst to contain the bed. Three thermocouples (K-type from Omega) were used to monitor the temperature in the reaction system. Thermocouples were placed in the inner tube of the reactor (before and after the catalyst sample), touching each end of the catalytic bed, as shown in Figure 1. The average of the temperatures recorded by these two thermocouples is reported as the reaction temperature. The maximum temperature difference between the two thermocouples was about five degrees. A thermocouple placed in the outer sleeve was used to control the reactor temperature via a PID controller on the reactor furnace.
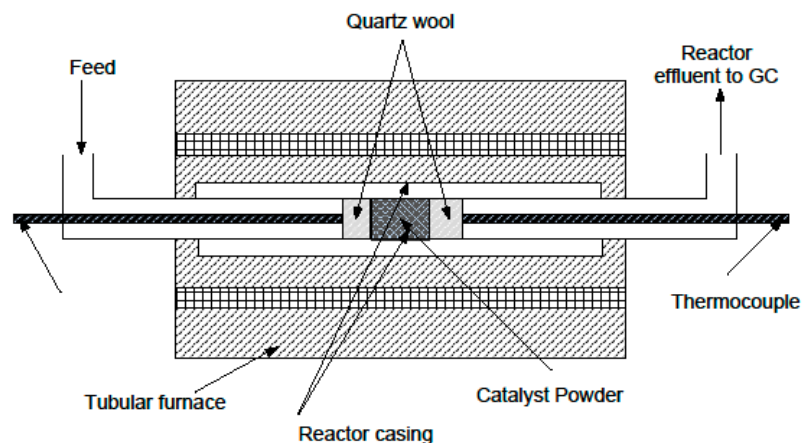
**Figure 1.** Schematic of the experimental reactor and furnace.

The reactor effluent was analyzed with a gas chromatograph (GC HP-7890-A type from Agilent Technologies Incorporation, Santa Clara, CA, USA). The GC column was 19095 P-Q4. The carrier gas was helium (ultra-high purity 5.0 from Praxair) with a flow rate of 11 cm³/min.

### 3.3. Reactor Feed Gas

The desired methane concentration was obtained by mixing 10 vol. % $CH_4$ in $N_2$ with extra dry air (Praxair, Allentown, PA, USA). Methane and air flow rates were controlled by flow meters in separate lines (line 1 for extra dry air controlled with a Matheson Modular DYNA blender model 8250 and line 2 for methane in nitrogen mixture controlled with an MKS Type 1479). The gases were mixed before entering the reactor.

When required, water was added using a peristaltic pump to give a feed fraction of 2%. Water was only used in the investigation of the commercial catalyst, denoted Catalyst 1. This level corresponds to the percentage of water vapour present in saturated air at 28 °C The reactor feed line was heated to avoid water condensation. All reported gas flow rates are based on 0 °C and 1 atm (STP). A total gas flow of 210 ± 5 mL$_{STP}$/min and 19.5 vol. % $O_2$ was used. This gas flow rate corresponds to a total molar flow rate of $F_T = 1.562 \times 10^{-4}$ mol/s. We note that the molar flow rate is constant because moles are conserved on reaction.

The experimental conditions and the temperature controller, GC, and water syringe pump system were controlled using LabVIEW NXG5.1 software connected to an Opto-22 system.

### 3.4. Experimental Procedure

The conversion vs. temperature data were obtained by measuring steady-state ignition curves. The reactor was started at a low temperature, and the temperature was then increased in a stepwise manner. At a series of pre-selected temperatures, the ramping was halted, and the outlet gas concentration was measured in triplicate. The fractional conversion was calculated from these values. The absolute reactor pressure was also measured at each data point. Ignition curves were obtained for the fresh catalyst and after several hydrothermal ageing cycles. Activities under wet and dry conditions were measured.
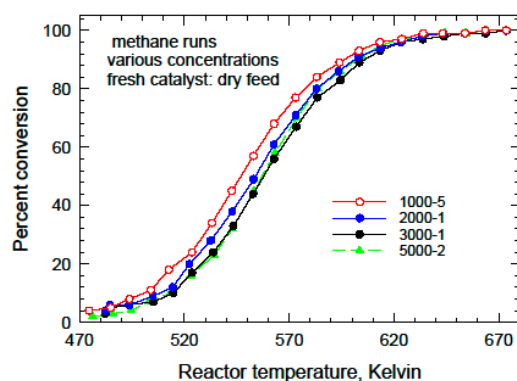
## 4. Experimental Ignition Curves

A complete set of all of the experimental ignition curves obtained during the investigation is given in the Supplementary Information for all of the catalysts used. In the main paper, we present sufficient information for the reader to understand the general behaviour. In the following sections, we present first the results obtained for Catalyst 1 followed by those obtained for the other five catalysts.

### 4.1. Ignition Curves for Commercial Catalyst, Catalyst 1

After the calcination step, ignition curves were obtained on the fresh catalyst at inlet methane concentrations of 1000, 2000, 3000, and 5000 ppm. The dry runs are shown in Figure 2 (also Figures S2 and S3). There is a systematic dependence of the conversion on the methane concentration. This effect is indicative of inhibition by water produced by combustion. Several runs were carried out for each methane concentration, and the results were repeatable. For simplicity, only a single curve is shown for each methane concentration.



**Figure 2.** Ignition curves for the fresh catalyst under dry conditions.

After the dry ignition experiments, the catalyst was hydrothermally aged (HTA-1) for 72 h at an overall flow rate of 210 mL/min (STP dry basis) with 5000 ppm methane and 2% water vapour. The temperature was 450 °C, with the temperature being lowered periodically to 285 °C to measure the activity, which is shown in Figure S4.

Following HTA-1, a set of ignition curves was measured in the absence of water. The activity was observed to be lower than that for the fresh catalyst (see Figure S5). Experiments performed with 1000 and 5000 ppm methane showed lower activity than for the fresh catalyst. Following these experiments, the catalyst was left for six weeks under air at room temperature. Following this period, the catalyst was heated in air to 450 °C and then cooled. Ignition curves were then obtained at 1000, 2000, 3000, and 5000 ppm methane. Figure S6 shows comparisons of the ignition curves obtained for the fresh catalyst, the catalyst immediately after HTA-1, and the catalyst after resting for six weeks. It was observed that the activity for each of these concentrations after the six-week rest had almost fully recovered to the level observed prior to the HTA. We have observed that the activity of Pd catalysts can recover somewhat after HTA when exposed to dry-reacting mixtures, but we have never tested over such a long time period. None of these runs for the "reactivated" was used in the subsequent kinetic analysis.

The catalyst was again hydrothermally aged (HTA-2) at 550 °C for 72 h. After cooling, ignition curves were obtained for 1000, 3000, and 5000 ppm methane with 2% water present in the feed. Experiments with dry feed were then performed at the same methane concentrations. The ignition curves are shown in Figure 3. We observed that the activity under dry conditions was lower than before, and the conversion depended on the inlet methane concentration. Under wet conditions, the conversion was apparently independent of the methane concentration.

A third hydrothermal ageing was performed, HTA-3, at 640 °C for 72 h. Ignition curves were obtained under wet and dry conditions. The results are shown in Figure 4. The overall trend is the same as that observed for the conversions obtained after HTA-2. After the completion of the dry tests, the catalyst was held for 60 h at a constant temperature of 350 °C (623 K) under dry conditions with 5000 ppm methane. The conversion showed a slow decrease during this time, giving a final conversion of about 73%.
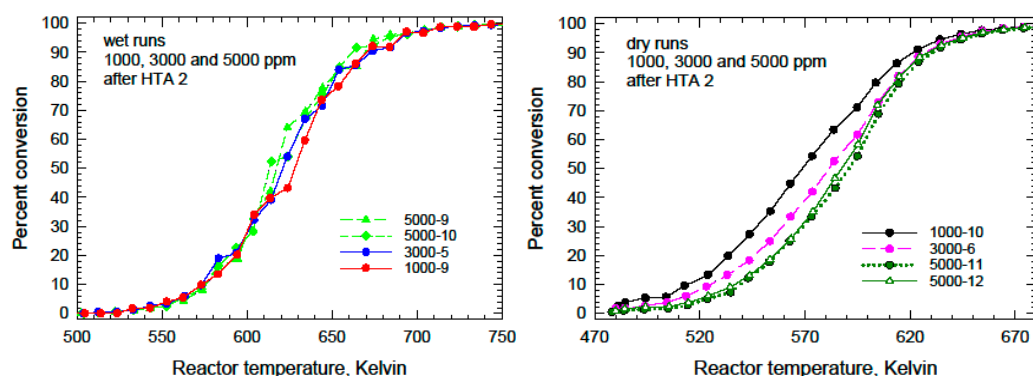
**Figure 3.** Wet (**left**) and dry (**right**) ignition curves after HTA number 2. The wet runs were performed first, and all curves were essentially the same. The dry runs were performed in the order 5000, 3000 1000, and then 5000 again.
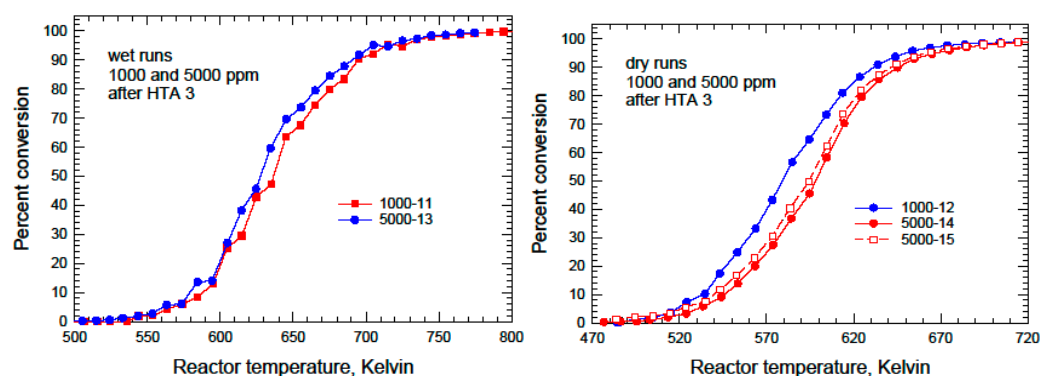


**Figure 4.** Wet (**left**) and dry (**right**) ignition curves after HTA-3. The wet runs were performed first, and all curves were essentially the same. The dry runs were performed in the order 5000, 1000, and then 5000 again.

A table of all of the experimental tests performed is given as Table S1 in the Supplementary Information, which also gives all of the experimental plots. We briefly summarize the main points from the experiments. In point form, they are as follows:

- The activity of the fresh catalyst under dry conditions was a bit erratic for the first two or three runs but then settled into reproducible behaviour.
- The ignition curves under dry conditions showed a consistent shift to the right, requiring a higher temperature for the same conversion, as the methane concentration increased. This behaviour can be attributed to the inhibition effects of water.
- The first hydrothermal ageing experiment showed a decrease in activity with time for HTA at 450 °C.
- The first dry ignition curves after HTA-1 showed lower activity than the fresh catalyst.
- After resting for six weeks, the dry activity of the catalyst returned to a value close to that observed for the fresh catalyst.
- During the second hydrothermal ageing (HTA-2) experiment, the activity was also seen to decline.
- Ignition curves taken after the HTA-2 experiment with wet feed were seen to be independent of the methane concentration, indicating an apparent first-order kinetics.
- Ignition curves taken under dry feed conditions showed lower activity than those measured after HTA-1.
- During the third hydrothermal ageing experiment, the activity also declined.
- Ignition curves taken under wet feed conditions were independent of the methane concentration, with lower activity than observed for wet runs after HTA-2.
- Dry runs after HTA-3 showed lower activity than the dry runs after HTA-2.

*4.2. Ignition Curves for Catalysts 2 to 6*

The ignition curves for Catalysts 2 to 6 considering all methane concentrations are given in the Supplementary Information as Figures S14–S18, and the significant curves are shown in Figure 5. Catalysts 2 and 4 show the least dependence on the methane concentration, whilst the other three show noticeable dependence, which suggests that water inhibition is important even at these low concentrations.
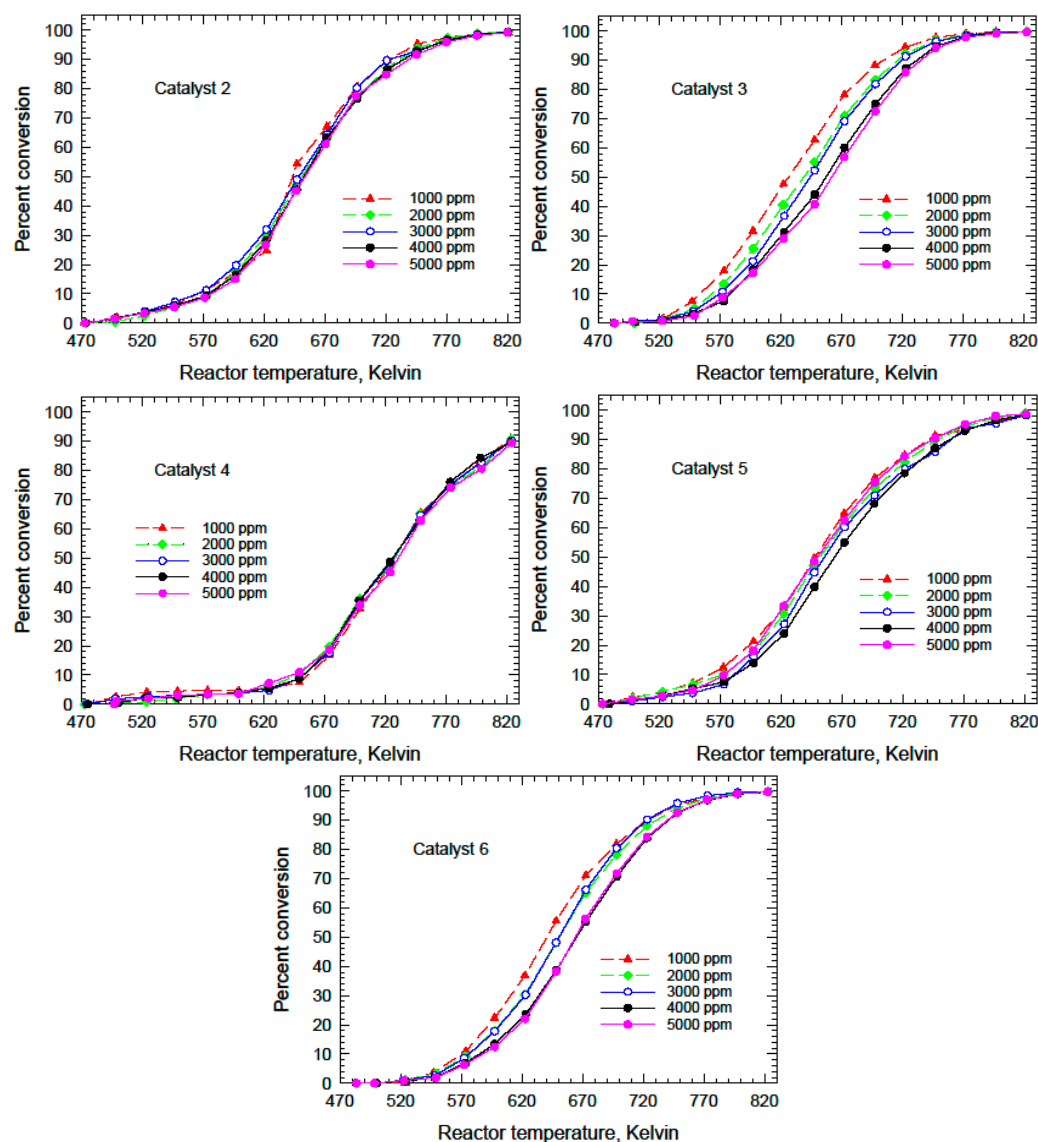
**Figure 5.** Ignition curves for catalysts 2 to 6 obtained for dry feed on fresh catalyst.

## 5. Kinetic Modelling

Kinetic modelling was performed on all of the reported catalysts. The modelling assumed an isothermal reactor, plug flow, and the absence of heat and mass transfer limitations. The maximum temperature rise across the catalyst bed was five degrees. The calculations validating the plug flow and heat and mass transfer assumptions are shown in detail in the Supplementary Information.

The main conclusion from the ignition curves is that the reaction is not overall first-order in the absence of added water for most of the catalysts. For Catalyst 1, with the addition of two percent by volume water, the reaction is apparently first-order overall. Clearly, the rate equation must involve a water inhibition term but one that dominates the denominator at high water concentrations. For the other catalysts, we have previously

reported their dependence on water [121,136]. In this section, we first present a detailed modelling study for Catalyst 1 with pseudo-first-order kinetics followed by a model that explicitly includes water inhibition. We then show the results of the same analysis for Catalysts 2 to 6.

As a preliminary step, the dry results were analyzed using a pseudo-first-order reaction, with the data at each feed concentration level being modelled separately. We assume that the reactor operated under isothermal plug flow conditions, and the rate constant is governed by an Arrhenius-type expression as follows:

$$k = \exp\left\{ A - E\left( \frac{1000}{R_g T} \right) \right\} \tag{13}$$

where $A$ is a constant, and $E$ is the activation energy in kJ/mol. We include the constant $A$ inside the exponential to improve the performance of the optimizer, which is a standard modelling trick. The Arrhenius plots for the dry runs for each methane concentration are given in Figure 6. There is an increasing trend in the apparent activation energy, which is indicative of the potential influence of water. The parameter values are given in Table 4.
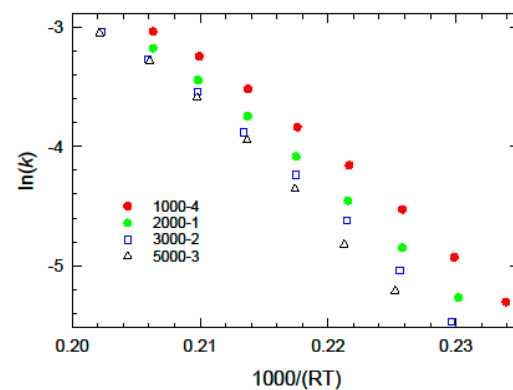


**Figure 6.** Arrhenius plots for the first-order reaction for the dry runs on the fresh catalyst (Catalyst 1).

**Table 4.** Summary of parameters obtained for the dry runs on the fresh catalyst.

| Run Details | $A$ | $E$ |
|---|---|---|
| 1000-4 | 14.19 | 83.06 |
| 2000-1 | 15.02 | 87.98 |
| 3000-2 | 15.21 | 89.68 |
| 5000-3 | 16.5 | 96.11 |

Now consider the effect of water explicitly, using an equation in the form of Equation (5).

$$(-r_{\mathrm{CH_4}}) = \frac{k\,[\mathrm{CH_4}]}{1 + K\,[\mathrm{CH_4}]} = \frac{\exp\left( A_0 - \frac{E}{R_g T} \right)[\mathrm{CH_4}]}{1 + K_0 \exp\left( \frac{H}{R_g T} \right)[\mathrm{CH_4}]} \tag{14}$$

For dry feed, the water concentration is directly related to the methane concentration and the fraction conversion, giving a rate model of the following form:

$$(-r_{\mathrm{CH_4}}) = \frac{k\left( F_{\mathrm{CH_4}} \right)_0 \left( 1 - X_{\mathrm{CH_4}} \right)}{Q\left( 1 + K\frac{2}{Q}\left( F_{\mathrm{CH_4}} \right)_0 X_{\mathrm{CH_4}} \right)} = \frac{k\left( F_{\mathrm{CH_4}} \right)_0 \left( 1 - X_{\mathrm{CH_4}} \right)}{\left( Q + 2K\left( F_{\mathrm{CH_4}} \right)_0 X_{\mathrm{CH_4}} \right)} \tag{15}$$

where $F$ denotes the molar flow rate, and $Q$ indicates the volumetric flow rate. If we assume plug flow and isothermal operation, then we can generate an analytical solution for fraction conversion. In terms of catalyst mass, the PFR mole balance is as follows:

$$\frac{d\,X_{CH_4}}{d\,W} \;=\; \frac{k\left(1 - X_{CH_4}\right)}{\left(Q + 2K\left(F_{CH_4}\right)_0 X_{CH_4}\right)} \tag{16}$$

The integration gives the following expression for the fraction conversion:

$$k\,W + \left(Q + 2K\left(F_{CH_4}\right)_0\right)\ln\left(1 - X_{CH_4}\right) + 2K\left(F_{CH_4}\right)_0 X_{CH_4} \;=\; 0 \tag{17}$$

An optimizer was built using MATLAB R2023b to determine the parameter values. Two optimization strategies were used, a genetic algorithm and one based on the gradient method. Both tools essentially gave the same results. Only the conversion data between 15% and 85% were used in the optimization. There were seven experiments performed under dry conditions on the fresh catalyst, and all seven were used to determine the optimal rate parameters. These parameters were found to be as follows:

$$k \;=\; \exp\left\{13.76 - 80.80\left(\frac{1000}{R_g T}\right)\right\} \qquad K \;=\; 0.0823\,\exp\left(21.29\left(\frac{1000}{R_g T}\right)\right) \tag{18}$$

A comparison of the experimental ignition curves and the model predictions for each inlet concentration of methane is shown in Figure 7. The agreement is satisfactory, especially in the conversion region above 20%.
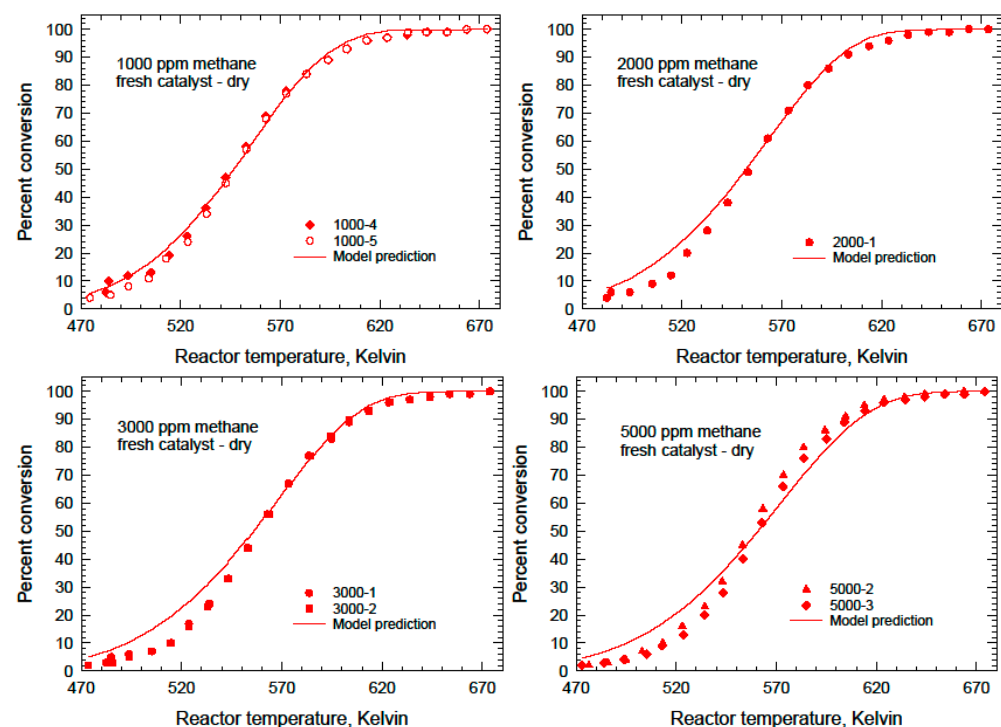


**Figure 7.** Comparison of experimental values to model predictions; generalized model for dry runs on the fresh catalyst.

The same optimization procedure was also performed for the dry runs obtained after HTA-1 (before the six-week break), HTA-2, and HTA-3. As before, only the data between 15% and 85% conversion were used. Five optimizations were performed in each case. In the first one, all four parameters in the kinetic model were allowed to vary. Then, the parameters were fixed successively to those obtained in the case of the fresh catalyst; that

is, first $H$ was fixed; then $H$ and $K_0$; then $H$, $K_0$, and $E$; and finally $H$ and $E$. The parameters are summarized in Table 5. The table gives the values when all parameters were free, as well as the values obtained when the values of $E$ and $H$ were fixed to be equal to the same value computed for the fresh catalyst, whilst the complete set is given in the Supplementary Information.

**Table 5.** Parameter values obtained for the optimization of the dry runs after each HTA. Parameters in bold red font were fixed during the optimization.

| Series | $A$ | $E$ | $K_0$ | $H$ |
| --- | --- | --- | --- | --- |
| Fresh | 13.76 | 80.80 | 0.0823 | 21.29 |
| After HTA-1 | | | | |
| Model (a) | 17.50 | 99.18 | 0.40 | 16.40 |
| Model (e) | 13.47 | **80.80** | 0.0873 | **21.29** |
| After HTA-2 | | | | |
| Model (a) | 17.19 | 99.13 | 0.01 | 36.77 |
| Model (e) | 13.10 | **80.80** | 0.108 | **21.29** |
| After HTA-3 | | | | |
| Model (a) | 16.79 | 99.46 | 0.0312 | 29.16 |
| Model (e) | 12.82 | **80.80** | 0.0840 | **21.29** |

Graphs of the agreements are presented in the Supplementary Information. The agreement between model and prediction is good in all cases. Although there are small differences obtained with each of the parameter sets, these differences are within the experimental uncertainty.

We can draw some overall conclusions regarding these dry runs. The first is that there is a range of parameter values that will give an acceptable fit, so the values shown should not necessarily be considered absolute. In particular, the model is fairly insensitive to the value of $H$, provided that the other parameters are allowed to adjust. Finally, it is interesting to observe that there is a set of common values for $E$, $K_0$, and $H$ that gives an acceptable fit for the four levels of catalyst activity, with only the value of $A$ being adjusted to reflect the deactivation. The comparisons are shown in Figures S22–S24.

We now consider the results when water was added to the feed. As shown earlier, the ignition curves obtained with 2% added water were essentially independent of the inlet methane concentration. Therefore, a first-order rate model is a close approximation for the result, because the water inhibition term in the denominator dominates the result. The first set of results to which a kinetic analysis was performed included the wet runs obtained after HTA-2. In the first instance, the kinetic parameters obtained using the Arrhenius analysis shown earlier were used to generate the ignition curves. The result is shown in Figure 8, denoted Model (a). As a second step, the first-order rate parameters were optimized using all of the data, including those at low and high concentrations. However, note that for this optimization, absolute errors were used to reduce the influence of the low and high conversion data. The resulting parameters were very similar, and the predicted ignition curve is also shown in Figure 8 as Model (b). The parameters for the two models are given in Table 6. As seen from both the graphs and the table of data, the results are very close in both cases.
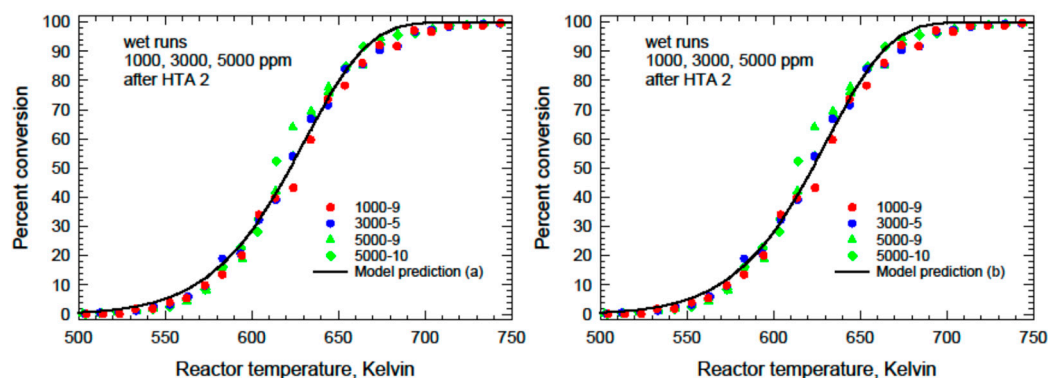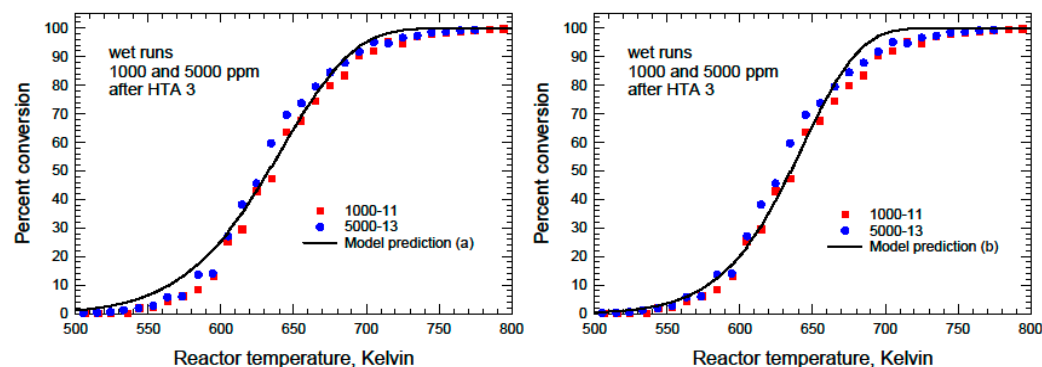
**Figure 8.** Predicted ignition curves for the wet runs obtained after HTA-2 for the two sets of model parameters. See Table 6.

**Table 6.** Parameters for the pseudo-first-order rate expression used for the runs with 2% water added, which were obtained after HTA-2.

| Model | A | E |
|---|---|---|
| Model (a) | 16.27 | 104.59 |
| Model (b) | 16.58 | 106.26 |

A similar analysis was performed on the wet ignition curves obtained after HTA-3, and the results are shown in Figure 9. In the first instance, the values obtained from the Arrhenius analysis performed earlier were used, denoted Model (a). Because the apparent activation energy obtained from the Arrhenius plot appeared to be much lower than expected, the data were optimized again by fixing the apparent activation energy to 104.59 kJ/mol, the value obtained for the wet runs after HTA-2. The optimization was carried out using the absolute error to calculate the objective function and both the data between 15% and 85% conversion and the entire dataset. The result was the same in both cases. This result is also shown in Figure 8 as Model (b). The parameter values are given in Table 7.



**Figure 9.** Predicted ignition curves for the wet runs obtained after HTA-3 for the three sets of model parameters. See Table 7.

**Table 7.** Parameters for the pseudo-first-order rate expression used for the runs with 2% water added, which were obtained after HTA-3 for the two models.

| Model | A | E |
|---|---|---|
| Model (a) | 12.33 | 85.48 |
| Model (b) | 15.90 | 104.59 |

We then repeated the analysis for Catalysts 2 to 6. The ignition data shown in Figure 5 were first analyzed in the same manner as for Catalyst 1, using in the first instance the pseudo-first-order approximation. The resulting Arrhenius style plots are shown in Figure 10; see also Figures S27–S31. The first-order rate parameters were determined by regression analysis for each methane concentration separately and for all of the data at all concentrations. The parameters thus obtained are shown in Table 8. The complex model with water inhibition, represented by Equation (14), was then optimized using the MATLAB program. The resulting parameters are given in Table 9.
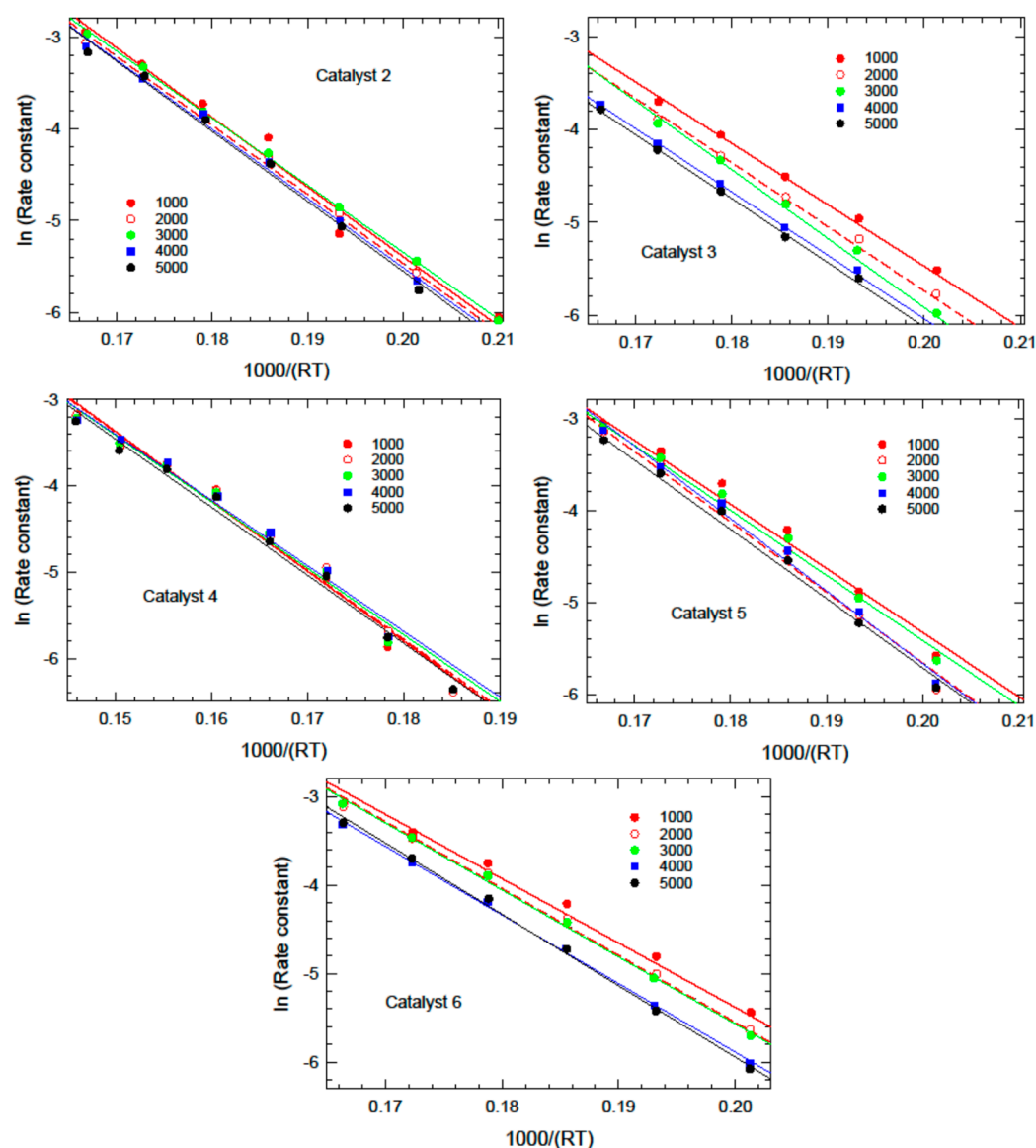


**Figure 10.** Arrhenius plots for the first-order reaction for the dry runs on fresh Catalysts 2 to 6.

Note that these parameters should not necessarily be considered unique. As seen for Catalyst 1 with the same complex rate model for the dry runs at different levels of catalyst activity, there are multiple sets of parameters that can give ignition curves that are virtually indistinguishable by the naked eye and have very small differences in the values of the objective function. For Catalysts 2 to 6, we let the MATLAB optimizer find the best values of the objective function and did not perform any sensitivity analysis on the parameter values. We are simply trying to show the differences between the fits that are possible with this complex model compared to the pseudo-first-order model.

**Table 8.** Summary of pseudo-first-order fitting for Catalysts 2 to 6. The activation energy has units of Kj/mol.

| Ppm | 1000 | 2000 | 3000 | 4000 | 5000 | all |
|---|---|---|---|---|---|---|
| | | | Catalyst 2 | | | |
| A | 9.74 | 9.54 | 9.24 | 9.53 | 9.67 | 9.48 |
| E | 75.6 | 75.0 | 72.9 | 75.2 | 76.1 | 74.6 |
| | | | Catalyst 3 | | | |
| A | 7.74 | 8.07 | 8.91 | 7.62 | 7.65 | 7.26 |
| E | 66.1 | 69.1 | 74.1 | 68.3 | 68.9 | 65.3 |
| | | | Catalyst 4 | | | |
| A | 8.79 | 8.63 | 8.16 | 8.02 | 8.4 | 8.46 |
| E | 81.1 | 80 | 77.1 | 76.1 | 79 | 79 |
| | | | Catalyst 5 | | | |
| A | 8.59 | 9.65 | 8.72 | 10.1 | 9.34 | 9.23 |
| E | 69.6 | 76.6 | 70.6 | 78.8 | 75.2 | 73.9 |
| | | | Catalyst 6 | | | |
| A | 9.16 | 9.58 | 9.58 | 9.62 | 10.2 | 9.22 |
| E | 72.7 | 75.7 | 75.7 | 77.5 | 80.7 | 73.9 |

**Table 9.** Summary of complex model fitting for Catalysts 2 to 6. The activation energy has units of Kj/mol.

| Catalyst | Composition | *A* | *E* | $K_0$ | *H* |
|---|---|---|---|---|---|
| 2 | Pd:Pt/$Co_3O_4$/$SnO_2$ | 10.6 | 79.9 | 2.18 | 1.81 |
| 3 | Pd:Pt/$SnO_2$ | 10.4 | 77.1 | 0.1 | 29.2 |
| 4 | Pd:Pt/$Co_3O_4$ | 8.6 | 79.3 | 0.812 | $1.0 \times 10^{-4}$ |
| 5 | Pd:Pt/$Co_3O_4$/$\gamma$-$Al_2O_3$ | 10.1 | 77.3 | 5.4 | $1.3 \times 10^{-4}$ |
| 6 | Pd:Pt/$\gamma$-$Al_2O_3$ | 10.0 | 75.4 | $4.1 \times 10^{-3}$ | 45.7 |

Figure 11 shows plots of the agreement of the model with the experimental results. For each catalyst, Figure 10 shows the agreement at a single concentration for both the first-order model and the complex model. In addition, the ignition curves at all of the concentration values were plotted, with either the first-order model (Catalysts 2, 4, and 5) or the complex model (Catalysts 3 and 6) fit. All of the curves are shown in the Supplementary Information, Figures S31–S35.

As mentioned earlier, detailed kinetic analysis for Catalysts 2 to 6 under high water feed conditions was reported in references [121,135]. We must emphasize that under high water conditions, all of the catalysts tested here showed strong water inhibition effects. To assist the discussion, we present a brief summary of the results below. For all of these catalysts, under conditions of either 5 or 10% water, there was negligible dependence on the methane concentration. This observation indicates that with large amounts of water in the feed, the relatively small amount of water produced by methane combustion does not exert a noticeable effect within the limits of the experimental error. In other words, at each water concentration level, the reaction appears to be first-order in methane. The apparent reaction order with respect to water can be determined by the analysis of the results at different water concentrations. These results are given in Table 10, where Model C1 refers to one with the form of Equation (5), while Model C2 has the form of Equation (9). We also show one result at 5 and 10% water for Catalyst 4, which shows apparent first-order behaviour at methane concentrations up to and including 5000 ppm by volume. Figure 12 shows the ignition curves.
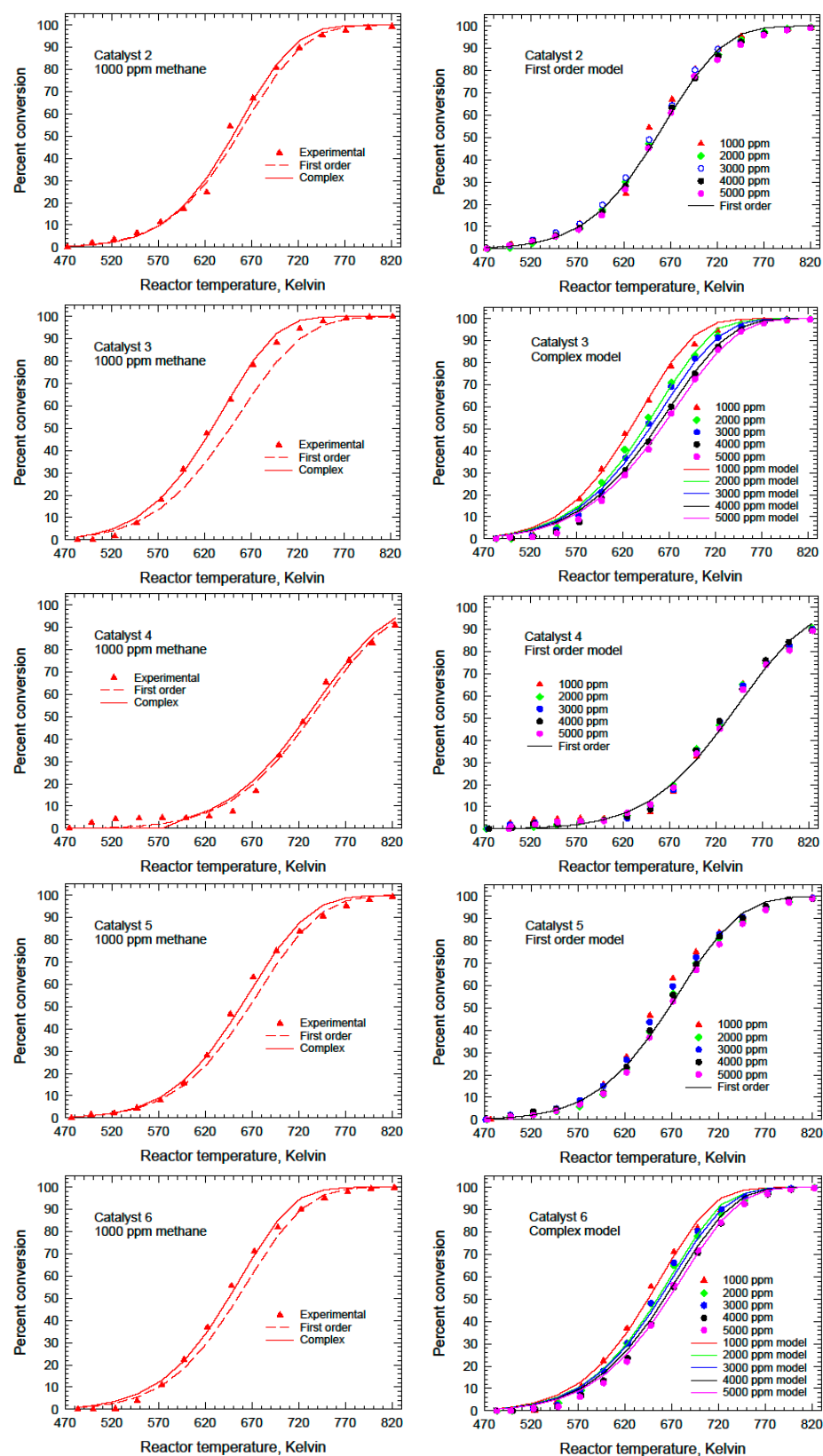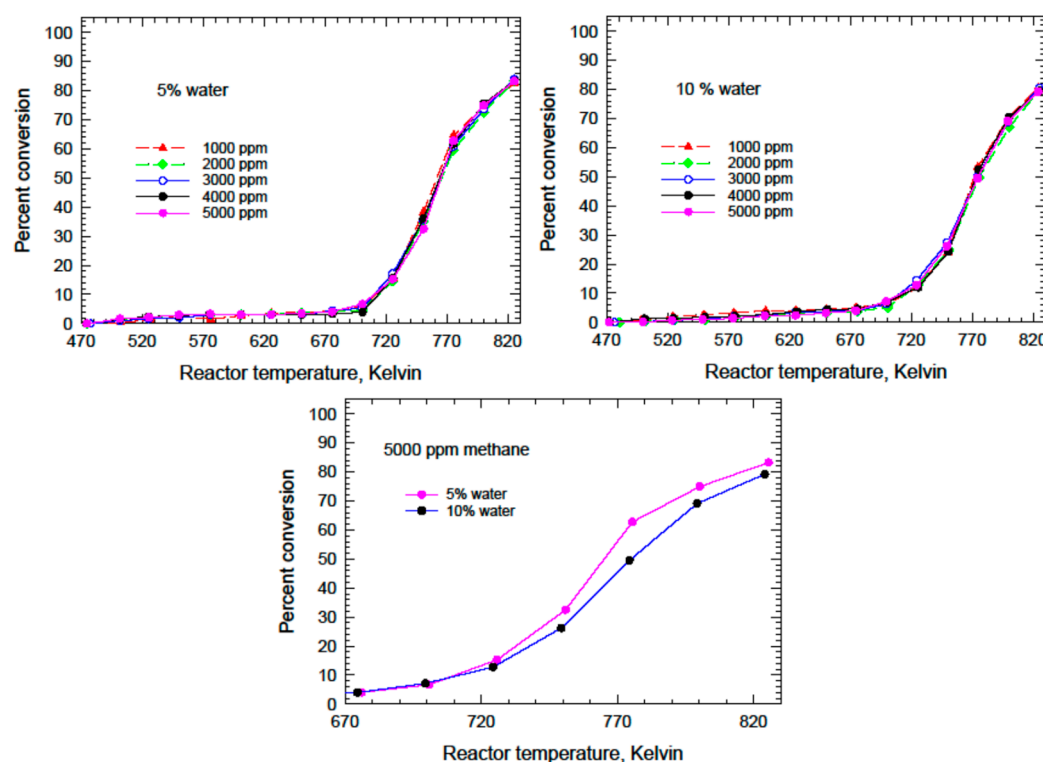
**Figure 11.** Agreement between model and experiment for Catalysts 2 to 6 in both models.

**Table 10.** Summary of the reaction dependence on water for Catalysts 2 to 6.

| Catalyst | Composition | Order WRT Water | Model | Ref |
|----------|-------------|-----------------|-------|-----|
| 2 | Pd:Pt/Co$_3$O$_4$/SnO$_2$ | $-0.37$ | C2 | [135] |
| 3 | Pd:Pt/SnO$_2$ | $-1$ | C1 | [121] |
| 4 | Pd:Pt/Co$_3$O$_4$ | $-0.42$ | C2 | [135] |
| 5 | Pd:Pt/Co$_3$O$_4$/$\gamma$-Al$_2$O$_3$ | $-0.55$ | C2 | [135] |
| 6 | Pd:Pt/$\gamma$-Al$_2$O$_3$ | $-1$ | C1 | [121] |



**Figure 12.** Effect of water concentration on activity for Catalyst 4.

## 6. Conclusions and Recommendations

It is evident from the literature presented here that there have been a wide variety of kinetic models presented for the catalytic combustion of methane over PGMs. Obviously, this literature covers a wide variety of catalyst formulations, including support types, promoters, and preparation techniques. The issue is complicated by the fact that complete catalyst details are sometimes lacking, and characterization data may not be available. Nevertheless, some observations can be made.

Water has an inhibiting effect on the catalyst activity; however, for some catalysts under dry feed conditions with low methane concentrations, a first-order model is sufficient. For the catalysts that we synthesized, the common denominator for the lack of water dependence at low methane concentration was the presence of cobalt in the support, that is, Catalysts 2, 4, and 5. That observation is consistent with the results presented in Table 10, where it is seen that the experiments conducted at high water concentrations showed a relatively low dependence on water, compared to Catalysts 3 and 6. At high water concentrations, a first-order model is often sufficient, although only at a specified feed water concentration. In other cases, even at low methane concentrations, the water effect is easily observable. What is certainly evident is that it is necessary to perform detailed kinetic measurements on any given catalyst to be certain that the result is valid, especially if one wishes to design a reactor based on the results.

One surprising result from the ageing studies on Catalyst 1 was the essentially complete recovery of the dry feed activity after the first hydrothermal ageing experiment when the catalyst was left for six weeks at ambient conditions. The recovery of activity after exposure to wet feed has been observed previously but never complete recovery. From a reactor operational standpoint, this observation may not be so significant, because operation would likely be either dry or wet only. However, it does emphasize the importance of the time scale when performing a mixture of wet and dry experiments to determine kinetics under deactivating conditions.

Considering Catalyst 1, we observed that for the dry and wet feed conditions, there was a common set of activation energies that gave an acceptable fit to the results at each deactivation level. However, better fits could be obtained when all parameters were allowed to vary, which is to be expected. One should always treat the actual values of parameters obtained in this manner with some level of caution and not state that one parameter set is necessarily better, simply because it gave a smaller value of the objective function.

As a final note, we emphasize the importance of computationally and experimentally determining the absence of mass and heat transfer limitation effects. While this advice is clearly well known, it can be difficult to achieve with rapid, highly exothermic combustion reactions, so special care should be taken.

**Data Availability Statement:** All experimental results obtained are shown in the Supplementary Information.

## References

1. Kesselring, J. Catalytic combustion. In *Advanced Combustion Methods*; Weinberg, J., Ed.; Academic Press: London, UK, 1986; pp. 237–275.
2. Prasad, R.; Kennedy, L.; Ruckenstein, E. Catalytic combustion. *Catal. Rev.—Sci. Eng.* **1984**, *29*, 219–267. [CrossRef]
3. Hayes, R.E.; Kolaczkowski, S.T. *Introduction to Catalytic Combustion*; Gordon and Breach Science Publishers: Reading, UK, 1997.
4. Sadamori, H. Application concepts and evaluation of small-scale catalytic combustors for natural gas. *Catal. Today* **1999**, *47*, 325–338. [CrossRef]
5. Etemad, S.; Karim, H.; Smith, L.; Pfefferle, W. Advanced technology catalytic combustor for high temperature ground power gas turbine applications. *Catal. Today* **1999**, *47*, 305–313. [CrossRef]
6. Forzatti, P. Status and perspectives of catalytic combustion for gas turbines. *Catal. Today* **2003**, *83*, 3–188. [CrossRef]
7. Kolios, G.; Gritsch, A.; Morillo, A.; Tuttlies, U.; Bernnat, J.; Opferkuch, F.; Eigenberger, G. Heat-integrated reactor concepts for catalytic reforming and automotive exhaust purification. *Appl. Catal. B Environ.* **2007**, *70*, 16–30. [CrossRef]
8. Kolios, G.; Frauhammer, J.; Eigenberger, G. Autothermal fixed-bed reactor concepts. *Chem. Eng. Sci.* **2000**, *55*, 5945–5967. [CrossRef]
9. Salamon, E.; Cornejo, I.; Mmbaga, J.P.; Kołodziej, A.; Lojewska, J.; Hayes, R.E. Investigations of a three-channel autogenous reactor for lean methane combustion. *Chem. Eng. Process. Process Intensif.* **2020**, *153*, 107956. [CrossRef]
10. Liu, B.; Hayes, R.E.; Mmbaga, J.; Yi, Y.; Checkel, M.D.; Zheng, M. Three-dimensional modelling of methane ignition in a reverse flow catalytic converter. *Comput. Chem. Eng.* **2007**, *31*, 292–306. [CrossRef]
11. Bernnat, J.; Rink, M.; Tuttlies, U.; Danner, T.; Nieken, U.; Eigenberger, G. Heat-integrated concepts for automotive exhaust purification. *Top. Catal.* **2009**, *52*, 2052–2057. [CrossRef]

12. Chen, J.; Arandiyan, H.; Gao, X.; Li, J. Recent advances in catalysts for methane combustion. *Catal. Surv. Asia* **2015**, *19*, 140–171. [CrossRef]

13. Cimino, S.; Di Benedetto, A.; Pirone, R.; Russo, G. Transient behaviour of perovskite-based monolithic reactors in the catalytic combustion of methane. *Catal. Today* **2001**, *69*, 95–103. [CrossRef]

14. Park, S.; Hwang, H.; Moon, J. Catalytic combustion of methane over rare earth stannate pyrochlore. *Catal. Lett.* **2003**, *87*, 219–223. [CrossRef]

15. Feng, S.; Wang, Z.; Yang, P. Effect of Substitution of Cobalt for Iron in Sr4Fe6O13-delta on the Catalytic Activity for Methane Combustion. *Chin. J. Chem.* **2011**, *29*, 451–454. [CrossRef]

16. Yang, J.; Guo, Y. Nanostructured perovskite oxides as promising substitutes of noble metals catalysts for catalytic combustion of methane. *Chin. Chem. Lett.* **2018**, *29*, 252–260. [CrossRef]

17. Zhu, W.; Jin, J.; Chen, X.; Li, C.; Wang, T.; Tsang, C.; Liang, C. Enhanced activity and stability of La-doped CeO2 monolithic catalysts for lean-oxygen methane combustion. *Environ. Sci. Pollut. Res.* **2018**, *25*, 5643–5654. [CrossRef] [PubMed]

18. Li, S.; Zhang, Y.; Wang, Z.; Du, W.; Zhu, G. Morphological effect of $CeO_2$ catalysts on their catalytic performance in lean methane combustion. *Chem. Lett.* **2020**, *49*, 461–464. [CrossRef]

19. Chen, J.; Zhang, X.; Arandiyan, H.; Peng, Y.; Chang, H.; Li, J. Low temperature complete combustion of methane over cobalt chromium oxides catalysts. *Catal. Today* **2013**, *201*, 12–18. [CrossRef]

20. Choya, A.; de Rivas, B.; González-Velasco, J.; Gutiérrez-Ortiz, J.; López-Fonseca, R. Oxidation of residual methane from VNG vehicles over Co3O4-based catalysts: Comparison among bulk, $Al_2O_3$-supported and Ce-doped catalysts. *Appl. Catal. B Environ.* **2018**, *237*, 844–854. [CrossRef]

21. Liotta, L.; Di Carlo, G.; Pantaleo, G.; Deganello, G. $Co_3O_4/CeO_2$ and $Co_3O_4/CeO_2$–$ZrO_2$ composite catalysts for methane combustion: Correlation between morphology reduction properties and catalytic activity. *Catal. Commun.* **2005**, *6*, 329–336. [CrossRef]

22. Cullis, C.F.; Willatt, B.M. Oxidation of methane over supported precious metal catalysts. *J. Catal.* **1983**, *83*, 267–285. [CrossRef]

23. Gélin, P.; Primet, M. Complete oxidation of methane at low temperature over noble metal based catalysts: A review. *App. Cat. B Environ.* **2002**, *39*, 1–37. [CrossRef]

24. Choudhary, T.; Banerjee, S.; Choudhary, V. Catalysts for combustion of methane and lower alkanes. *Appl. Catal. A Gen.* **2002**, *234*, 1–23. [CrossRef]

25. Ciuparu, D.; Lyubovsky, M.; Altman, E.; Pfefferle, L.; Datye, A. Catalytic combustion of methane over palladium-based catalysts. *Catal. Rev.—Sci. Eng.* **2002**, *44*, 593–649. [CrossRef]

26. Monai, M.; Montini, T.; Gorte, R.; Fornasiero, P. Catalytic Oxidation of Methane: Pd and Beyond. *Eur. J. Inorg. Chem.* **2018**, *25*, 2884–2893. [CrossRef]

27. Becker, E.; Carlsson, P.A.; Grönbeck, H.; Skoglundh, M. Methane oxidation over alumina supported platinum investigated by time-resolved in situ XANES spectroscopy. *J. Catal.* **2007**, *252*, 11–17. [CrossRef]

28. Deutschmann, O.; Maier, L.; Riedel, U.; Stroemman, A.; Dibble, R. Hydrogen assisted catalytic combustion of methane on platinum. *Catal. Today* **2000**, *59*, 141–150. [CrossRef]

29. Bui, P.; Vlachos, D.; Westmoreland, P. Catalytic ignition of methane/oxygen mixtures over platinum surfaces: Comparison of detailed simulations and experiments. *Surf. Sci.* **1997**, *385*, L1029–L1034. [CrossRef]

30. Deutschmann, O.; Behrendt, F.; Warnatz, J. Modeling and simulation of heterogeneous oxidation of methane on a platinum foil. *Catal. Today* **1994**, *21*, 461–470. [CrossRef]

31. Reinke, M.; Mantzaras, J.; Bombach, R.; Schenker, S.; Yylli, N. Effects of $H_2O$ and $CO_2$ Dilution on the Catalytic and Gas-Phase Combustion of Methane, over Platinum at Elevated Pressures. *Combust. Sci. Technol.* **2006**, *179*, 553–600. [CrossRef]

32. Mazzarino, I.; Barresi, A. Catalytic combustion of VOC mixtures in a monolith reactor. *Catal. Today* **1993**, *17*, 335–348. [CrossRef]

33. Niwa, M.; Awano, K.; Murakami, Y. Activity of supported platinum catalysts for methane oxidation. *Appl. Catal.* **1983**, *7*, 317–325. [CrossRef]

34. O'Connell, M.; Kolb, G.; Zapf, R.; Men, Y.; Hessel, V. Bimetallic catalysts for the catalytic combustion of methane using microreactor technology. *Catal. Today* **2009**, *144*, 306–311. [CrossRef]

35. Trimm, D.; Lam, C. The combustion of methane on platinum-alumina fibre catalysts I Kinetics and Mechanism. *Chem. Eng. Sci.* **1980**, *35*, 1405–1413. [CrossRef]

36. Jodeiri, N.; Wu, L.; Mmbaga, J.; Hayes, R.E.; Wanke, S.E. Catalytic Combustion of VOC in a Counter-diffusive Reactor. *Catal. Today* **2010**, *155*, 147–153. [CrossRef]

37. Cullis, C.; Nevell, T.; Trimm, D. Role of the catalyst support in the oxidation of methane over palladium. *J. Chem. Soc. Faraday Trans. 1 Phys. Chem. Condens. Phases* **1972**, *68*, 1406–1412. [CrossRef]

38. Schwartz, W.; Ciuparu, D.; Pfefferle, L. Combustion of methane over palladium-based catalysts: Catalytic deactivation and role of the Support. *J. Phys. Chem. C* **2012**, *116*, 8587–8593. [CrossRef]

39. Schwartz, W.; Pfefferle, L.D. Combustion of methane over palladium-based catalysts: Support interactions. *J. Phys. Chem. C* **2012**, *116*, 8571–8578. [CrossRef]

40. Escandon, L.; Ordonez, S.; Vega, A.; Diez, F. Oxidation of methane over palladium catalysts: Effect of the support. *Chemosphere* **2005**, *58*, 9–17. [CrossRef] [PubMed]

41. Kumar, R.; Hayes, R.; Semagina, N. Effect of support on Pd-catalyzed methane-lean combustion in the presence of water: Review. *Catal. Today* **2021**, *382*, 82–95. [CrossRef]

42. Garbowski, E.; Feumi-Jantou, C.; Mouaddib, N.; Primet, M. Catalytic combustion of methane over palladium supported on alumina catalysts: Evidence for reconstruction of particles. *Appl. Catal. A Gen.* **1994**, *109*, 277–292. [CrossRef]

43. Friberg, I.; Sadokhina, N.; Olsson, L. Complete methane oxidation over Ba modified Pd/$Al_2O_3$: The effect of water vapour. *Appl. Catal. B Environ.* **2018**, *231*, 242–250. [CrossRef]

44. Demoulin, O.; Navez, M.; Ruiz, P. Investigation of the behavior of a Pd/$\gamma$-$Al_2O_3$ catalyst during methane combustion reaction using in situ DRIFT spectroscopy. *Appl. Catal. A Gen.* **2005**, *295*, 59–70. [CrossRef]

45. Demoulin, O.; Navez, M.; Gaigneaux, E.; Ruiz, P.; Mamede, A.; Granger, P.; Payen, E. Operando resonance Raman spectroscopic characterisation of the oxidation state of palladium in Pd/g-$Al_2O_3$ catalysts during the combustion of methane. *Phys. Chem. Chem. Phys.* **2003**, *5*, 4394–4401. [CrossRef]

46. Datye, A.; Bravo, J.; Nelson, T.; Atanasova, P.; Lyubovsky, M.; Pfefferle, L. Catalyst microstructure and methane oxidation reactivity during the Pd-PdO transformation on alumina supports. *Appl. Catal. A Gen.* **2000**, *198*, 179–196. [CrossRef]

47. Ciuparu, D.; Perkins, E.; Pfefferle, L. In situ DR-FTIR investigation of surface hydroxyls on -$Al_2O_3$ supported PdO catalysts during methane combustion. *Appl. Catal. A Gen.* **2004**, *263*, 145–153. [CrossRef]

48. Castellazzi, P.; Groppi, G.; Forzatti, P.; Baylet, A.; Marecot, P.; Duprez, D. Role of Pd loading and dispersion on redox behaviour and $CH_4$ combustion activity of $Al_2O_3$ supported catalysts. *Catal. Today* **2010**, *155*, 18–26. [CrossRef]

49. Hicks, R.; Qi, H.; Young, M.; Lee, R. Effect of catalyst structure on methane oxidation over palladium on alumina. *J. Catal.* **1990**, *122*, 295–306. [CrossRef]

50. Hong, E.; Kim, C.; Lim, D.; Cho, H.; Shin, C. Catalytic methane combustion over Pd/$ZrO_2$ catalysts: Effects of crystalline structure and textural properties. *Appl. Catal. B Environ.* **2018**, *232*, 544–552. [CrossRef]

51. Guerrero, S.; Araya, P.; Wolf, E. Methane oxidation on Pd supported on high area zirconia catalysts. *Appl. Catal. A Gen.* **2006**, *298*, 243–253. [CrossRef]

52. Fujimoto, F.; Ribiero, R.; Avalos Borja, A.; Iglesia, E. Structure and reactivity of $PdO_x$/$ZrO_2$ catalysts for methane oxidation at low temperatures. *J. Catal.* **1998**, *179*, 431–442. [CrossRef]

53. Carstens, J.; Su, S.; Bell, A. Factors Affecting the Catalytic Activity of Pd/ZrO2 for the Combustion of Methane. *J. Catal.* **1998**, *176*, 136–142. [CrossRef]

54. Ibashi, W.; Groppi, G.; Forzatti, P. Kinetic measurement of $CH_4$ combustion over a 10% PdO/$ZrO_2$ catalyst using an annular flow micro reactor. *Catal. Today* **2003**, *83*, 115–129. [CrossRef]

55. Araya, P.; Guerrero, S.; Robertson, J.; Gracia, F. Methane combustion over Pd/$SiO_2$ catalysts with different degrees of hydrophobicity. *Appl. Catal. A Gen.* **2005**, *283*, 225–233. [CrossRef]

56. Bassil, J.; Al Barazi, A.; Da Costa, P.; Boutros, M. Catalytic combustion of methane over mesoporous silica supported palladium. *Catal. Today* **2011**, *176*, 36–40. [CrossRef]

57. Hoyos, L.; Praliaud, H.; Primet, M. Catalytic combustion of methane over palladium supported on alumina and silica in presence of hydrogen sulfide. *Appl. Catal. A Gen.* **1993**, *98*, 125–138. [CrossRef]

58. Gannouni, A.; Albela, B.; Said Zina, M.; Bonneviot, L. Metal dispersion, accessibility and catalytic activity in methane oxidation of mesoporous templated aluminosilica supported palladium. *Appl. Catal. A Gen.* **2013**, *464–465*, 116–127. [CrossRef]

59. Ercolino, G.; Grzybek, G.; Stelmachowski, P.; Specchia, S.; Kotarba, A.; Specchia, V. Pd/Co3O4-based catalysts prepared by solution combustion synthesis for residual methane oxidation in lean conditions. *Catal. Today* **2015**, *257*, 66–71. [CrossRef]

60. Li, Z.; Xu, G.; Hoflund, G. In situ IR studies on the mechanism of methane oxidation over Pd/$Al_2O_3$ and Pd/$Co_3O_4$ catalysts. *Fuel Process. Technol.* **2003**, *84*, 1–11. [CrossRef]

61. Hoffmann, M.; Kreft, S.; Georgi, G.; Fulda, G.; Pohla, M.; Seeburg, D.; Berger-Karin, C.; Kondratenko, E.; Wohlrab, S. Improved catalytic methane combustion of Pd/$CeO_2$ catalysts via porous glass integration. *Appl. Catal. B Environ.* **2015**, *179*, 313–320. [CrossRef]

62. Lei, Y.; Li, W.; Liu, Q.; Lin, Q.; Zhenga, X.; Huanga, Q.; Guan, S.; Wanga, X.; Wang, C.; Li, F. Typical crystal face effects of different morphology ceria on the activity of Pd/$CeO_2$ catalysts for lean methane combustion. *Fuel* **2018**, *233*, 10–20. [CrossRef]

63. Huang, Q.; Li, W.; Lei, Y.; Guan, S.; Zheng, X.; Pan, Y.; Wen, W.; Zhu, J.; Zhang, H.; Lin, Q. Catalytic Performance of Novel Hierarchical Porous Flower-Like $NiCo_2O_4$ Supported Pd in Lean Methane Oxidation. *Catal. Lett.* **2018**, *148*, 2799–2811. [CrossRef]

64. Roth, D.; Gelin, P.; Tena, E.; Primet, M. Combustion of methane at low temperature over Pd and Pt catalysts supported on $Al_2O_3$, $SnO_2$ and $Al_2O_3$-grafted $SnO_2$. *Top. Catal.* **2001**, *16*, 77–82. [CrossRef]

65. Urfels, L.; Gelin, P.; Primet, M.; Tena, E. Complete oxidation of methane at low temperature over Pt catalysts supported on high surface area $SnO_2$. *Top. Catal.* **2004**, *30*, 427–432. [CrossRef]

66. Kinnunen, N.; Suvanto, M.; Moreno, M.; Savimaki, A.; Kallinen, K.; Kinnunen, T.; Pakkanen, T. Methane oxidation on alumina supported palladium catalysts: Effect of Pd precursor and solvent. *Appl. Catal. A Gen.* **2009**, *370*, 78–87. [CrossRef]

67. Lu, Y.; Michalow, K.; Matam, S.; Winkler, A.; Maeglia, A.; Yoona, S.; Heele, A.; Weidenkaffa, A.; Ferri, D. Methane abatement under stoichiometric conditions on perovskite-supported palladium catalysts prepared by flame spray synthesis. *Appl. Catal. B Environ.* **2014**, *144*, 631–643. [CrossRef]

68. Lu, Y.; Eyssler, A.; Otala, E.; Matam, S.; Brunko, O.; Weidenkaff, A.; Ferri, D. Influence of the synthesis method on the structure of Pd-substituted perovskite catalysts for methane oxidation. *Catal. Today* **2013**, *208*, 42–47. [CrossRef]

69. Auvray, X.; Lindholm, A.; Milh, M.; Olsson, L. The addition of alkali and alkaline earth metals to Pd/Al2O3 to promote methane combustion. Effect of Pd and Ca loading. *Catal. Today* **2018**, *299*, 212–218. [CrossRef]

70. Colussi, S.; Trovarelli, A.; Cristiani, C.; Lietti, L.; Groppi, G. The influence of ceria and other rare earth promoters on palladium-based methane combustion catalysts. *Catal. Today* **2012**, *180*, 124–130. [CrossRef]

71. Kang, T.; Kim, J.; Kang, S.; Seo, G. Promotion of methane combustion activity of Pd catalyst by titania loading. *Catal. Today* **2000**, *59*, 87–93. [CrossRef]

72. Bounechada, D.; Groppi, G.; Forzatti, P.; Kallinen, K.; Kinnunen, T. Effect of periodic lean/rich switch on methane conversion over a Ce–Zr promoted Pd-Rh/Al2O3 catalyst in the exhausts of natural gas vehicles. *Appl. Catal. B Environ.* **2012**, *119–120*, 91–99. [CrossRef]

73. Ersson, A.; Kušar, H.; Carroni, R.; Griffin, T.; Järås, S. Catalytic combustion of methane over bimetallic catalysts a comparison between a novel annular reactor and a high-pressure reactor. *Catal. Today* **2003**, *83*, 265–277. [CrossRef]

74. Kul Ryu, C.; Wong Ryoo, M.; Soo Ryu, I.; Kang, S. Catalytic combustion of methane over supported bimetallic Pd catalysts: Effects of Ru or Rh addition. *Catal. Today* **1999**, *47*, 141–147. [CrossRef]

75. Lyubovsky, M.; Smith, L.; Castaldi, M.; Karim, H.; Nentwick, B.; Etemad, S.; LaPierre, R.; Pfefferle, W. Catalytic combustion over platinum group catalysts: Fuel-lean versus fuel-rich operation. *Catal. Today* **2003**, *83*, 71–84. [CrossRef]

76. Oh, S.; Mitchell, P. Effects of rhodium addition on methane oxidation behavior of alumina-supported noble metal catalysts. *Appl. Catal. B Environ.* **1994**, *5*, 165–179. [CrossRef]

77. Yang, N.; Liu, J.; Sun, Y.; Zhu, Y. Au@PdOx with a PdOx-rich shell and Au-rich core embedded in $Co_3O_4$ nanorods for catalytic combustion of methane. *Nanoscale* **2019**, *9*, 4108–4109. [CrossRef] [PubMed]

78. Venezia, A.; Murania, R.; Pantaleo, G.; Deganello, G. Pd and PdAu on mesoporous silica for methane oxidation: Effect of $SO_2$. *J. Catal.* **2007**, *251*, 94–102. [CrossRef]

79. Miao, S.; Deng, Y. Au-Pt/$Co_3O_4$ catalyst for methane combustion. *Appl. Catal. B Environ.* **2001**, *31*, l1–l4. [CrossRef]

80. Lapisardi, G.; Urfels, L.; Gelin, P.; Primet, M.; Kaddouri, A.; Garbowski, E.; Toppi, S.; Tena, E. Superior catalytic behaviour of Pt-doped Pd catalysts in the complete oxidation of methane at low temperature. *Catal. Today* **2006**, *117*, 564–568. [CrossRef]

81. Lapisardi, G.; Gélin, P.; Kaddouri, A.; Garbowski, E.; Da Costa, S. Pt-Pd bimetallic catalysts for methane emissions abatement. *Top. Catal.* **2007**, *42*, 461–464. [CrossRef]

82. Kinnunen, N.; Hirvi, J.; Suvanto, M.; Pakkanen, T. Methane combustion activity of Pd–PdOx–Pt/$Al_2O_3$ catalyst: The role of platinum promoter. *J. Mol. Catal. A Chem.* **2012**, *356*, 20–28. [CrossRef]

83. Bugosh, G.; Easterling, V.; Rusakova, I.; Harold, M. Anomalous steady-state and spatio-temporal features of methane oxidation on Pt/Pd/$Al_2O_3$ monolith spanning lean and rich condition. *Appl. Catal. B Environ.* **2015**, *165*, 68–78. [CrossRef]

84. Watanabe, T.; Kawashima, K.; Tagawa, Y.; Tashiro, K.; Anoda, H.; Ichioka, K.; Sumiya, S.; Zhang, G. New DOC for light duty diesel DPF system. In *SAE Technical Paper Series*; 2007-01-1920; SAE International: Warrendale, PA, USA, 2007.

85. Nomura, K.; Noro, K.; Nakamura, Y.; Yazawa, Y.; Yoshida, H.; Satsuma, A.; Hattori, T. Pd–Pt bimetallic catalyst supported on SAPO-5 for catalytic combustion of diluted methane in the presence of water vapor. *Catal. Lett.* **1998**, *53*, 167–169. [CrossRef]

86. Persson, K.; Jansson, K.; Järås, S. Characterisation and microstructure of Pd and bimetallic Pd–Pt catalysts during methane oxidation. *J. Catal.* **2007**, *245*, 401–414. [CrossRef]

87. Nassiri, H.; Hayes, R.E.; Semagina, N. Stability of Pd-Pt catalysts in low-temperature wet methane combustion: Metal ratio and particle reconstruction. *Chem. Eng. Sci.* **2018**, *186*, 44–51. [CrossRef]

88. Goodman, E.; Dai, S.; Yang, A.; Wrasman, C.; Gallo, A.; Bare, S.; Hoffman, A.; Jaramillo, T.; Graham, G.; Pan, X.; et al. Uniform Pt/Pd Bimetallic Nanocrystals Demonstrate Platinum Effect on Palladium Methane Combustion Activity and Stability. *ACS Catal.* **2017**, *7*, 4372–4380. [CrossRef]

89. Persson, K.; Ersson, A.; Jansson, K.; Fierro, J.; Jaras, S. Influence of molar ratio on Pd–Pt catalysts for methane combustion. *J. Catal.* **2006**, *243*, 14–24. [CrossRef]

90. Yamamoto, H.; Uchida, H. Oxidation of methane over Pt and Pd supported on alumina in lean-burn natural-gas engine exhaust. *Catal. Today* **1998**, *45*, 147–151. [CrossRef]

91. Semagina, N.; Nassiri, H.; Lee, K.; Hu, Y.; Hayes, R.E.; Scott, R.W.J. Water shifts PdO-catalyzed lean methane combustion to Pt-catalyzed rich combustion in Pd-Pt catalysts: In-situ X-ray absorption spectroscopy. *J. Catal.* **2017**, *352*, 649–656.

92. Nassiri, H.; Lee, K.; Hu, Y.; Hayes, R.E.; Scott, R.W.J.; Semagina, N. Platinum inhibits low-temperature dry lean methane combustion via palladium reduction in Pd-Pt/$Al_2O_3$: An in-situ X-ray absorption study. *ChemPhysChem* **2017**, *18*, 238–244. [CrossRef]

93. Chen, M.; Schmidt, L.D. Morphology and composition of Pt-Pd alloy crystallites on $SiO_2$ in reactive atmospheres. *J. Catal.* **1979**, *56*, 198–218. [CrossRef]

94. Campbell, C.T.; Foyt, D.C.; White, J.M. Oxygen penetration into the bulk of palladium. *J. Phys. Chem.* **1977**, *81*, 491–494. [CrossRef]

95. Chen, J.J.; Ruckenstein, E. Role of interfacial phenomena in the behaviour of alumina-supported palladium crystallites in oxygen. *J. Phys. Chem.* **1981**, *85*, 1606–1612. [CrossRef]

96. Farrauto, R.J.; Hobson, M.C.; Kennelly, T.; Waterman, E.M. Catalytic chemistry of supported palladium for combustion of methane. *Appl. Catal. A Gen.* **1992**, *81*, 227–237. [CrossRef]

97. Lyubovsky, K.; Pfefferle, L. Methane combustion over the alpha-alumina supported Pd catalyst: Activity of the mixed Pd/PdO state. *Appl. Catal. A Gen.* **1998**, *173*, 107–119. [CrossRef]

98.  Lyubovsky, K.; Pfefferle, L. Complete methane oxidation over Pd catalyst supported on alpha-alumina. Influence of temperature and oxygen pressure on the catalyst activity. *Catal. Today* **1999**, *47*, 29–44.

99.  Van Den Bossche, M.; Grönbeck, H. Methane Oxidation over PdO(101) Revealed by First-Principles Kinetic Modeling. *J. Amer. Chem. Soc.* **2015**, *137*, 12035–12044. [CrossRef]

100.  Xin, Y.; Lieb, S.; Wang, H.; Law, C.K. Kinetics of Catalytic Oxidation of Methane over Palladium Oxide by Wire Microcalorimetry. *J. Phys. Chem. C* **2013**, *117*, 19499–19507. [CrossRef]

101.  Specchia, S.; Conti, F.; Specchia, V. Kinetic Studies on Pd/CexZr1−xO2 Catalyst for Methane Combustion. *Ind. Eng. Chem. Res.* **2010**, *49*, 11101–11111. [CrossRef]

102.  Müller, C.A.; Maciejewski, M.; Koeppel, R.A.; Tschan, R.; Baiker, A. Role of Lattice Oxygen in the Combustion of Methane over PdO/ZrO2: Combined Pulse TG/DTA and MS Study with 18O-Labeled Catalyst. *J. Phys. Chem.* **1996**, *100*, 20006–20014. [CrossRef]

103.  Centi, G. Supported Palladium Catalysts in Environ. Catalytic Technologies for Gaseous Emissions. *J. Mol. Catal. A Chem.* **2001**, *173*, 287–312. [CrossRef]

104.  Hayes, R.E.; Kolaczkowski, S.T.; Li, P.K.C.; Awdry, S. The Palladium Catalysed Oxidation of Methane: Reaction Kinetics and the Effect of Diffusion Barriers. *Chem. Eng. Sci.* **2001**, *56*, 4815–4835. [CrossRef]

105.  Ciuparu, D.; Pfefferle, L.D. Support and Water Effects on Palladium Based Methane Combustion Catalysts. *Appl. Catal. A Gen.* **2001**, *209*, 415–428. [CrossRef]

106.  Ribeiro, F.H.; Chow, M.; Dalla Betta, R.A. Kinetics of the Complete Oxidation of Methane over Supported Palladium Catalysts. *J. Catal.* **1994**, *146*, 537–544. [CrossRef]

107.  Burch, R.; Crittle, D.J.; Hayes, M.J. C-H Bond Activation in Hydrocarbon Oxidation on Heterogeneous Catalysts. *Catal. Today* **1999**, *47*, 229–234. [CrossRef]

108.  Cullis, C.F.; Willatt, B.M. The inhibition of hydrocarbon oxidation over supported precious metal catalysts. *J. Catal.* **1984**, *86*, 187–200. [CrossRef]

109.  Burch, R.; Urbano, F.J.; Loader, P.K. Methane combustion over palladium catalysts—The effect of carbon-dioxide and water on activity. *Appl. Catal. A Gen.* **1995**, *123*, 173–184. [CrossRef]

110.  Card, R.J.; Schmitt, J.L.; Simpson, J.M. Palladium-carbon hydrogenolysis catalysts: The effect of preparation variables on catalytic activity. *J. Catal.* **1983**, *79*, 13–20. [CrossRef]

111.  Baldwin, T.R.; Burch, R. Catalytic Combustion of Methane over Supported Palladium Catalysts: I. Alumina Supported Catalysts. *Appl. Catal.* **1990**, *66*, 337–358. [CrossRef]

112.  Otto, K. Methane Oxidation over Pt on 7-Alumina: Kinetics and Structure Sensitivity. *Langmuir* **1989**, *21*, 1364–1369. [CrossRef]

113.  Marti, P.E.; Maciejewski, M.; Baiker, A. Methane oxidation over palladium on zirconia prepared from amorphous Pd1ZR3 alloy. *J. Catal.* **1993**, *139*, 495–509. [CrossRef]

114.  Cullis, C.F.; Keene, D.E.; Trimm, D.L. Pulse flow reactor studies of the oxidation of methane over palladium catalysts. *J. Chem. Soc. Faraday Trans.* **1971**, *67*, 864–876. [CrossRef]

115.  Qi, W.; Ran, J.; Wang, R.; Du, X.; Shi, J.; Niu, J.; Zhang, P.; Ran, M. Kinetic Consequences of Methane Combustion on Pd, Pt and Pd–Pt Catalysts. *RSC Adv.* **2016**, *6*, 109834–109845. [CrossRef]

116.  Golodets, G.I. *Heterogeneous Catalytic Reactions Involving Molecular Oxygen*; Elsevier: Amsterdam, The Netherlands, 1983.

117.  Mezaki, R.; Watson, C.C. Catalytic Oxidation of Methane. *Ind. Eng. Chem. Proc. Des. Dev.* **1966**, *5*, 62–65. [CrossRef]

118.  Kikuchi, R.; Maeda, S.; Sasaki, K.; Wennerström, S.; Eguchi, K. Low-Temperature Methane Oxidation over Oxide-Supported Pd Catalysts: Inhibitory Effect of Water Vapor. *Appl. Catal. A Gen.* **2002**, *232*, 23–28. [CrossRef]

119.  Hicks, R.F.; Qi, H.; Young, M.L.; Lee, R.G. Structure Sensitivity of Methane Oxidation over Platinum and Palladium. *J. Catal.* **1990**, *122*, 280–294. [CrossRef]

120.  Alyani, M.; Smith, K.J. Kinetic Analysis of the Inhibition of CH4 Oxidation by H2O on PdO/Al2O3 and CeO2/PdO/Al2O3 Catalysts. *Ind. Eng. Chem. Res.* **2016**, *55*, 8309–8318. [CrossRef]

121.  Kumar, R.S.; Hayes, R.E.; Semagina, N. Pd and Pd-Pt Catalysts Supported on SnO2 and γ-Al2O3: Kinetic Studies of Wet Lean Methane Combustion. *Chem. Eng. Sci.* **2023**, *269*, 118488. [CrossRef]

122.  Keller, K.; Lott, P.; Tischer, S.; Casapu, M.; Grunwaldt, J.-D.; Deutschmann, O. Methane Oxidation over PdO: Towards a Better Understanding of the Influence of the Support Material. *ChemCatChem* **2023**, *15*, e202300366. [CrossRef]

123.  Nasr, S.; Semagina, N.; Hayes, R.E. Kinetic Modelling of Co3O4- and Pd/Co3O4-Catalyzed Wet Lean Methane Combustion. *Emiss. Control. Sci. Technol.* **2020**, *6*, 269–278. [CrossRef]

124.  Abbasi, R.; Wu, L.; Wanke, S.E.; Hayes, R.E. Kinetics of Methane Combustion over Pt and Pt–Pd Catalysts. *Chem. Eng. Res. Des.* **2012**, *90*, 1930–1942. [CrossRef]

125.  Deutschmann, O.; Behrendt, F.; Warnatz, J. Formal Treatment of Catalytic Combustion and Catalytic Conversion of Methane. *Catal. Today* **1998**, *46*, 155–163. [CrossRef]

126.  Boşomoiu, M.; Bozga, G.; Soare, G. Methane Combustion Over a Commercial Platinum on Alumina Catalyst: Kinetics and Catalyst Deactivation. *Rev. Roum. Chim.* **2008**, *53*, 1105–1115.

127.  Burch, R.; Loader, P.K.; Urbano, F.J. Some Aspects of Hydrocarbon Activation on Platinum Group Metal Combustion Catalysts. *Catal. Today* **1996**, *27*, 243–248. [CrossRef]

128. Neomagus, H.W.J.P.; Saracco, G.; Wessel, H.F.W.; Versteeg, G.F. The Catalytic Combustion of Natural Gas in a Membrane Reactor with Separate Feed of Reactants. *Chem. Eng. J.* **2000**, *77*, 165–177. [CrossRef]

129. Habibi, A.H.; Semagina, N.; Hayes, R.E. Kinetics of Low-Temperature Methane Oxidation over $SiO_2$ -Encapsulated Bimetallic Pd-Pt Nanoparticles. *Ind. Eng. Chem. Res.* **2018**, *57*, 8160–8171. [CrossRef]

130. Yang, Y.; Lee, J.; Dorakhan, R.; Nie, H.; Fu, G.; Quarantotto, A.; Howe, J.Y.; Chin, Y.H. (Cathy) Active Site Structure and Methane Oxidation Reactivity of Bimetallic Pd and Pt Nanoparticles. *Appl. Catal. A Gen* **2022**, *629*, 118290. [CrossRef]

131. Kolaczkowski, S.T.; Thomas, W.J.; Titiloye, J.; Worth, D.J. Catalytic combustion of methane in a monolith reactor: Heat and mass transfer under laminar flow and pseudo-steady-state reaction conditions. *Combust. Sci. Technol.* **1996**, *118*, 79–100. [CrossRef]

132. Hayes, R.E.; Kolaczkowski, S.T.; Thomas, W.J.; Titiloye, J. Transient experiments and modelling of the catalytic combustion of methane in a monolith reactor. *Ind. Eng. Chem. Res.* **1996**, *35*, 406–414. [CrossRef]

133. Sakai, T.; Chol, B.C.; Osuga, R.; Ko, Y. *Purification Characteristics of Catalytic Converters for Natural Gas Fuelled Automotive Engine*; SAE: Warrendale, PA, USA, 1991; p. 912599.

134. Liu, B.; Hayes, R.E.; Checkel, M.D.; Zheng, M.; Mirosh, E. Reversing flow catalytic converter for a natural gas/diesel dual fuel engine. *Chem. Eng. Sci.* **2001**, *56*, 2641–2658. [CrossRef]

135. Kumar, R.S.; Hayes, R.E.; Semagina, N. Kinetic investigation of the promoting effect of cobalt on Pd-Pt/SnO2 catalyzed wet methane combustion. *Appl. Catal. A Gen.* **2023**, *666*, 119416. [CrossRef]

136. Abbasi, R.; Huang, G.; Istratescu, G.M.; Wu, L.; Hayes, R.E. Methane oxidation over Pt, Pt:Pd and Pd based catalysts: Effects of pre-treatment. *Can. J. Chem. Eng.* **2015**, *93*, 1474–1482. [CrossRef]

137. Dautzenberg, F.M. *Ten Guidelines for Catalyst Testing*; American Chemical Society: Washington, DC, USA, 1989; pp. 99–119. [CrossRef]

138. Dry Air Properties [WWW Document], n.d. Available online: https://www.engineeringtoolbox.com/dry-air-properties-d_973.html (accessed on 8 May 2024).

139. Fogler, S. *Elements of Chemical Reaction Engineering*, 5th ed.; 2011; Available online: https://www.academia.edu/43355099/Elements_of_Chemical_Reaction_Engineering_Fifth_edition_pdf (accessed on 8 May 2024).

140. Fuller, E.N.; Schettler, P.D.; Giddings, J.C. A new method for prediction of binary gasphase diffusion coefficients. *Ind. Eng. Chem.* **1966**, *58*, 18–27. [CrossRef]

141. Hayes, R.E.; Mmbaga, J.P. *Introduction to Chemical Reactor Analysis*, 2nd ed.; Taylor and Francis Group, CRC Press: Boca Raton, FL, USA, 2012.

142. Lyons, W.; Plisga, G.; Lorenz, M. *Standard Handbook of Petroleum and Natural Gas Engineering*, 3rd ed.; Elsevier: Amsterdam, The Netherlands, 2016.